A system of feed-forward cerebellar circuits that extend and diversify sensory signaling

Harsh N. Hariani[1,3], A. Brynn Algstam[2,3], Christian T. Candler[1,3], Isabelle F. Witteveen[3], Jasmeen K. Sidhu[3] & Timothy S. Balmer[3*]

1) Interdisciplinary Graduate Program in Neuroscience

2) Barrett Honors College

3) School of Life Sciences, Arizona State University, Tempe, AZ, 85287

*corresponding Author: timothy.balmer@asu.edu

ABSTRACT

Sensory signals are processed by the cerebellum to coordinate movements. Numerous cerebellar functions are thought to require the maintenance of a sensory representation that extends beyond the input signal. Granule cells receive sensory input, but they do not prolong the signal and are thus unlikely to maintain a sensory representation for much longer than the inputs themselves. Unipolar brush cells (UBCs) are excitatory interneurons that project to granule cells and transform sensory input into prolonged increases or decreases in firing, depending on their ON or OFF UBC subtype. Further extension and diversification of the input signal could be produced by UBCs that project to one another, but whether this circuitry exists is unclear. Here we test whether UBCs innervate one another and explore how these small networks of UBCs could transform spiking patterns. We characterized two transgenic mouse lines electrophysiologically and immunohistochemically to confirm that they label ON and OFF UBC subtypes and crossed them together, revealing that ON and OFF UBCs innervate one another. A Brainbow reporter was used to label UBCs of the same ON or OFF subtype with different fluorescent proteins, which showed that UBCs innervate their own subtypes as well. Computational models predict that these feed-forward networks of UBCs extend the length of bursts or pauses and introduce delays—transformations that may be necessary for cerebellar functions from modulation of eye movements to adaptive learning across time scales.

SIGNIFICANCE STATEMENT

The cerebellum is essential for the accurate performance of behaviors ranging in complexity from stabilizing an image on the retina to playing a piano or performing a gymnastics routine. Cerebellar dysfunction disrupts the ability to produce smooth movements and leads to a disorder called ataxia. Damage to the vestibular cerebellum occurs in various disorders including medulloblastoma and leads to nystagmus, involuntary movements of the eyes that prevent normal vision. Treating disorders of motor control such as nystagmus, requires a better understanding of how representations of movements are maintained in the firing patterns of neurons in the cerebellar circuit. Here we use transgenic mice to label a type of neuron called the unipolar brush cell and revealed that these cells innervate one another and are likely to increase the length and diversity of spiking patterns in the cerebellum. These transformations may be necessary for numerous functions from controlling eye movements to learning new behaviors.

INTRODUCTION

Head movement signals are encoded by the firing rate of vestibular afferents that project to the cerebellum and brainstem. The vestibular nuclei maintain a sensory representation of the head movement for tens of seconds after the vestibular signal ends through a mechanism called velocity storage (Fernandez and Goldberg, 1971; Raphan et al., 1979). The cerebellum dynamically modulates the activity of the cells that encode velocity storage to control vestibular responses such as compensatory eye movements (Yakushin et al., 2017). It is unclear how the cerebellar circuit maintains a representation of a head movement long after the firing of the afferents cease.

Granule cells receive direct input from vestibular afferents, but cannot maintain the signal long enough to underlie velocity storage, because they produce only transient firing responses. The only other excitatory neuron type in the cerebellar cortex that could provide feed-forward excitation to prolong the signal to granule cells is the unipolar brush cell (UBC). UBCs are powerful circuit elements that amplify their input signals by extending them in time and projecting them to numerous granule cells (Berthie and Axelrad, 1994; Mugnaini et al., 1994, 2011; Rossi et al., 1995; Nunzi et al., 2001). UBCs receive direct input from vestibular afferents, produce long duration spiking responses, and could therefore contribute to the maintenance of a sensory representation necessary to modulate low-frequency vestibular responses (Rossi et al., 1995; Mugnaini et al., 2011; Balmer and Trussell, 2019). Although a single UBC can prolong its input for seconds, multiple UBCs connected in series could extend the signal much further. Indeed, there is some evidence suggesting that UBCs provide direct synaptic input to other UBCs (Diño et al., 2000; Nunzi and Mugnaini, 2000; van Dorp and De Zeeuw, 2015).

In addition to prolonging signals, UBCs may play important roles in diversifying granule cell firing patterns, which is essential for expansion recoding models of cerebellar learning (Marr, 1969; Albus, 1971; Ito, 1982; Kennedy et al., 2014). This diversity in UBC responses is due to different subtypes of UBCs that can be classified by their expression of specific proteins or neurotransmitter receptors (Nunzi et al., 2002, 2003; Kim et al., 2012; Sekerkova et al., 2014) or by their electrophysiological response to synaptic stimulation: ON UBCs that express mGluR1 are excited by glutamate and OFF UBCs that express calretinin are inhibited by glutamate (Borges-Merjane and Trussell, 2015). Whether UBCs target UBCs of their own subtype, the other, or both, remains unclear, and is necessary to understand how sensory signals are extended and diversified in the granule cell layer.

The connectivity of different types of UBCs is difficult to address. Paired electrophysiological recordings of synaptically connected UBCs are challenging because of their long axons and their relative scarcity among the granule cells. Labeling UBCs of the same type with a single fluorophore provides ambiguous results- the axon terminals of UBCs look similar to UBC dendritic brushes, so a UBC axon contacting a dendritic brush of the same color would appear essentially identical to a large brush. We overcame this challenge by utilizing a Brainbow approach and by combining mouse lines to label UBC subtypes with different fluorescent proteins. We find that all UBC connectivity patterns are present and develop computational models to simulate how these feed-forward circuits dynamically transform their inputs. Interconnected UBCs prolong and diversify input spiking patterns by producing an extended burst (ON to ON), extended pause (ON to OFF), pause after a delay (OFF to ON), or burst after a delay (OFF to OFF). Thus, UBCs connected in series increase the computational power of the circuit and could underlie mechanisms of cerebellar function that require transmission delays or prolonged activity.

RESULTS

Electrophysiological responses of GRP and P079 UBCs reveal that they are ON and OFF UBC subtypes

To label a population of UBCs that are excited by glutamate (ON UBCs), we used a mouse line that expressed Cre recombinase (Cre) under the control of the GRP (gastrin releasing peptide) promoter (Gerfen et al., 2013), a promoter that had been reported to be active in mGluR1-expressing (mGluR1(+)) UBCs in a similar mouse line (Kim et al., 2012). We crossed the GRP-Cre mouse to a tdTomato reporter (Ai9) (Madisen et al., 2010) and targeted fluorescently labeled UBCs for whole-cell recording in acute brain slices (Fig 1A). The white matter of lobe X was stimulated with an extracellular electrode to evoke synaptic currents.

Synaptic stimulation evoked fast EPSCs and a slow inward current that began at the end of stimulation at higher frequencies, which is diagnostic of ON UBCs (n = 15) (Fig 1B). The latency between presynaptic stimulation and the beginning of the fast EPSC was 1.24 ± 0.29 ms (mean ± SD; n = 13), had a low jitter (defined as the SD of latency; 0.074 ± 0.046 ms; mean ± SD; n = 13), and was reliable, having no failures across all cells and trials, which confirms that they were monosynaptic. Note that these monosynaptic currents are most likely due to the stimulation of mossy fibers, but could also be due to stimulation of severed axons of UBCs. The slow EPSCs peaked 70.13 ± 33.45 ms after the end of the 200 ms long 50 Hz stimulus train and their decay was well approximated by an exponential with a time constant of 358.31 ± 213.83 ms (mean ± SD; n = 14) (Fig 1C). In current-clamp recordings, synaptic stimulation produced a burst of action potentials in GRP UBCs that varied in duration from 510 to 900 ms (n = 3) (Fig 1D). The synaptic currents in GRP UBCs were confirmed to be mediated by mGluR1 and AMPA receptors because they were blocked by JNJ16259685 and GYKI53655 (99.3 ± 2.4%; paired t-test; P=0.0068; n = 9; mean ± SEM) (Fig 1E-F). While the two drugs together blocked most of the inward current (Fig 1F), their individual contribution ranged widely in different cells (3-70% block by JNJ16259685 and 30-100% block by GYKI53655). This indicates that GRP UBCs are ON UBCs and their synaptic responses vary from being mediated mainly by mGluR1 to being entirely mediated by AMPA receptors.

Using the same approach, we tested the response to synaptic stimulation in a population of UBCs that expressed mCitrine in a mouse line (P079) that was generated in an enhancer trap forward genetic screen (Shima et al., 2016). In all P079 UBCs recorded that responded to presynaptic stimulation, a 50 Hz train evoked a slow outward current (n = 12). Faster rates of synaptic stimulation produced larger outward currents (Fig 1G). The slow outward currents peaked 52.7 ± 46.86 ms after the end of the 200 ms long 50 Hz stimulus train and their decay was well approximated by an exponential with a time constant of 489.2 ± 350.4 ms (mean ± SD; n = 11) (Fig 1H). These outward currents hyperpolarized the cells and produced a pause in spontaneous spiking activity that varied from 0.5 to 3.9 seconds, averaging 1.72 ± 1.19 seconds (mean ± SD; n = 10) (Fig 1I). The outward current was mediated by mGluR2 receptors, as it was blocked by the mGluR2 antagonist LY341495 (96.53 ± 1.79%; paired t-test; P=0.0033; mean ± SEM) (Fig 1J-K). These electrophysiological characteristics confirm that the P079 UBCs that can be visualized in acute brains slices are OFF UBCs.

The slow postsynaptic currents were inward in every GRP UBCs and outward in every P079 UBC (Fig 1L). The capacitance of GRP UBCs was less than half that of P079 UBCs, which suggests that the

membrane area of the OFF UBCs is greater (GRP UBCs: 11.34 pF ± 0.59, n = 15; P079 UBCs: 26.08 pF ± 1.96, n = 12; t-test; P<0.0001; mean ± SEM; Fig 1M). We did not observe a significant difference in input resistance between the two cell types (GRP UBCs: 0.56 GΩ ± 0.04, n = 9; P079 UBCs: 0.64 GΩ ± 0.09, n = 10; t-test; P = 0.44; mean ± SEM; Fig 1N). Current steps were injected into both UBC types to characterize their excitability. There was a significant interaction between the UBC type and response to current steps (mixed model ANOVA, P<0.0001, n = 17). GRP UBCs had a higher firing rate in response to the same level of injected current compared to P079 UBCs, despite their similar input resistance, suggesting that GRP ON UBCs are more excitable and can fire at faster rates (Fig 1O-P). Hyperpolarizing current steps produce a sag that is mediated by the h-current (Ih) in UBCs (Kim et al., 2012). P079 UBCs had a significantly more prominent sag than GRP UBCs, measured in response to a -100-pA current step (peak/steady state; P079: 1.69 ± 0.13, n = 7; GRP: 1.19 ± 0.02, n=14; t-test; P<0.0001; mean ± SEM) (Fig 1P-Q). This is consistent with previous work showing that OFF UBCs have a larger h-current than ON UBCs (Kim et al., 2012). In summary, electrophysiological recordings from GRP and P079 UBCs confirm that they are ON and OFF UBC subtypes, respectively.

GRP and P079 UBCs are distinct subpopulations that differ in size and distribution

Besides the functional differences in the GFP and mCitrine-expressing UBCs outlined above, these neurons also showed significant differences in their size and distribution. Crossing the GRP-Cre/Ai9 mice with the P079 mice resulted in triple transgenic mice that expressed tdTomato and mCitrine in almost entirely separate subpopulations of UBCs—only 3 out of 944 UBCs that were labeled expressed both fluorescent proteins. GRP and P079 UBCs were present in the lobes of the cerebellar vermis in different densities (Fig 2A). More GRP UBCs than P079 UBCs were present in lobes VI-IX, with few of either type in lobes II-V. The highest density of both UBC types was in lobe X, which is where we focused the following analyses (Fig 2B). UBCs have convoluted dendritic brushes that are similar in appearance to their axon terminals (Fig 2C).

GRP UBCs have been reported to have smaller somas than UBCs that express calretinin (calretinin(+)), a calcium-binding protein that labels the OFF UBC population (Kim et al., 2012; Borges-Merjane and Trussell, 2015). We found that the cross-sectional area of GRP UBCs was significantly smaller than that of P079 UBCs (GRP: 68.75 ± 9.69 μm^2, mean ± SD, n = 92; P079: 74.47 ± 12.53 μm^2, mean ± SD, n = 114, t-test, P = 0.0004), which is consistent with our electrophysiological analysis of their membrane capacitance (Fig 2D). The distribution of GRP and P079 UBCs also supports their identity as ON and OFF UBCs, as the density of mGluR1(+) ON UBCs is higher in the dorsal leaflet of lobe X and the density of calretinin(+) OFF UBCs is higher in the ventral leaflet (Nunzi et al., 2002; Sekerkova et al., 2014).

GRP UBCs are a subset of mGluR1(+) UBCs

Somatodendritic expression of mGluR1 and calretinin defines two separate populations of UBCs (termed Type II and Type I, respectively (Nunzi et al., 2002)) and correspond to the functionally-defined ON and OFF subtypes (Borges-Merjane and Trussell, 2015). To investigate the expression of mGluR1 and calretinin in GRP and P079 UBCs, we immunohistochemically labeled, imaged, and counted UBCs in both

162 ventral and dorsal areas of lobe X in 4-8 brain slices from triple transgenic mice (n = 4 mice). We found
163 that 98.1% (155/158) of the GRP/Ai9 UBCs expressed mGluR1 in their dendritic brushes (Fig 3A-B). The
164 GRP/Ai9/mGluR1(+) population represented 20.9% (155/741) of the total population of mGluR1(+)
165 UBCs. 0/149 GRP/Ai9 UBCs expressed calretinin in a separate series of slices (Fig 3C-D). Thus, the GRP
166 line labels about 1/5th of the ON UBCs and does not label OFF UBCs.

167

168 ***P079 mouse line drives mCitrine expression in the majority of calretinin(+) UBCs***

169 Using the same triple transgenic mice and immunohistochemical approach described above,
170 92.2% (284/308) of the P079 UBCs were calretinin(+) (Fig 3C-D). The P079 UBCs represent 70.5%
171 (284/403) of the total calretinin(+) population. We were surprised to find, however, that 61.3%
172 (200/326) of the P079 UBCs appeared mGluR1(+). This represents 27.0% (200/741) of the total
173 mGluR1(+) population. These P079/mGluR1(+) UBCs could be differentiated from P079/mGluR1(-) UBCs
174 by their lower expression of mCitrine: the relative labeling intensity of the mGluR1(+) P079 UBCs, after
175 amplification with an anti-GFP antibody, was less than half of the more common mGluR1(-) P079 UBCs
176 (43.2% soma pixel intensity relative to mGluR1(-) P079 UBCs, n = 34 z-planes with at least one of each
177 type, t-test, P = 8.403e-6). In addition, the cross-sectional area of the mGluR1(+) P079 somas was 60.62
178 ± 13.67 μm^2, mean ± SD, n = 52 and significantly smaller than the mGluR1(-) P079 somas (72.48 ± 16.90
179 μm^2 mean ± SD, n = 40, t-test, P = 0.00035). It is likely that the P079 UBCs that express a low density of
180 mCitrine were not able to be visualized in our electrophysiological experiments because their native
181 fluorescence was below the level of detection. Unfortunately, the observation that some mGluR1(+)
182 UBCs are labeled in the P079 mouse line precludes its use for expressing genes in OFF UBCs specifically.

183

184 ***GRP and P079 UBCs are distinct populations in dorsal cochlear nucleus***

185 UBCs are also present in the dorsal cochlear nucleus, a cerebellum-like circuit in the auditory
186 brainstem of mammals. Like granule cells in the dorsal cochlear nucleus, UBCs receive multisensory
187 signals from various sources (Ryugo et al., 2003; Balmer and Trussell, 2021, 2022). In order to test
188 whether our findings about the identity of UBCs labeled in GRP-cre and P079 mice is generalizable
189 across UBC populations, we examined their distribution in the dorsal cochlear nucleus. We found that
190 97.8% (132/135) of the GRP/Ai9 UBCs expressed mGluR1 in their dendritic brushes (Fig 4A-B). The
191 GRP/Ai9/mGluR1(+) population represented 34.2% (132/386) of the population of mGluR1(+) UBCs, and
192 is therefore a subpopulation of about 1/3 of the mGluR1(+) ON UBCs. In a separate series of slices,
193 0/115 GRP/Ai9 UBCs expressed calretinin and is therefore useful for expressing genes in a subset of ON
194 UBCs without expression in OFF UBCs in the dorsal cochlear nucleus.

195 We also found that 89.7% (140/156) of the P079 UBCs were calretinin(+) (Fig 4C-D). The P079
196 UBCs represent 85.9% (140/163) of the total calretinin(+) population. Similar to our results in the
197 cerebellum, we found that 56.7% (127/224) of the P079 UBCs were mGluR1(+). This represents 32.9%
198 (127/386) of the mGluR1(+) population. As in the cerebellum, these P079/mGluR1(+) UBCs were
199 identifiable by their significantly lower intensity of mCitrine after antibody amplification (43.5% intensity
200 compared to mGluR1(-) P079 UBCs, n = 19 z-planes with at least one of each type, t-test, P = 1.352e-6).
201 In summary, in the dorsal cochlear nucleus, the P079 mouse line expresses mCitrine in 86% of the

202 calretinin(+) UBCs and 33% of the mGluR1(+) UBCs and the GRP line expresses Cre in 34% of the
203 mGluR1(+) UBC population and 0% of the calretinin(+) population. Thus, the expression pattern in the
204 dorsal cochlear nucleus of UBCs in these two mouse lines mirrors that of the cerebellum.

205

206 ***Axonal projections between ON UBCs and OFF UBCs***

207 Do ON and OFF UBC subtypes target one another? In the GRP/Ai9/P079 mouse line, all GRP
208 UBCs are ON UBCs and the P079 UBCs are mostly OFF UBCs, although their OFF UBC identity must be
209 confirmed by their expression of calretinin. Thus, we searched for red GRP UBC axon terminals that
210 contacted green P079 UBC brushes that also expressed calretinin. These contacts were presumed to be
211 synapses based on our previous anatomical analyses of functional synapses between mossy fibers and
212 UBCs (Balmer and Trussell, 2019). Several examples of such synaptic connections were identified,
213 indicating that GRP ON UBCs provide synaptic input to P079 OFF UBCs (Fig 5A-B). Using the same
214 approach, we found OFF UBC axon terminals (P079 and calretinin(+)) contacting ON UBC brushes (GRP)
215 (Fig 5C-D). These projections were rare and we did not attempt to characterize the proportion of ON to
216 OFF UBC connections, as both populations are subsets of ON and OFF UBCs and would be a significant
217 underestimate. However, these results do reveal that UBC subtypes synapse on one another and may
218 introduce complex spiking patterns.

219

220 ***Axonal projections from ON UBCs to other ON UBCs***

221 To test whether ON UBCs synapse on other ON UBCs, we searched for labeled axon terminals in
222 the GRP/Ai9 mouse that contacted brushes of ON UBCs labeled with mGluR1. Two examples are shown
223 in Fig 6. Care was taken to confirm that mGluR1 labeling that appeared to decorate the brush of a UBC
224 could be traced to a soma with the characteristic expression in the somatic membrane that forms a
225 circle. These examples show that GRP ON UBCs target mGluR1(+) UBCs that are not transgenicially
226 labeled in the GRP mouse line.

227 In a second approach to investigate synaptic connections between ON UBCs, we utilized a
228 Brainbow2.1-Confetti reporter mouse line to label GRP ON UBCs with distinct colors (Livet et al., 2007;
229 Snippert et al., 2010). In the offspring resulting from the GRP-Cre/Brainbow2.1-Confetti cross,
230 expression of the fluorescent proteins was low and it was therefore necessary to enhance with anti-GFP
231 and anti-mCherry antibodies. In doing so, both membrane-bound mCerulean and cytoplasmic YFP were
232 labeled with the anti-GFP antibody, and cytoplasmic tdimer2(12) was labeled with anti-mCherry. This
233 resulted in various combinations of expression that could be identified by wavelength (green or red) and
234 cellular localization (membrane-bound or cytoplasmic). In most labeled UBCs, multiple alleles were
235 expressed and could be visualized in the same cells, perhaps owing to the sensitivity of the antibody
236 amplification (Fig 7A). Several examples of GRP UBC axon terminals contacting the brushes of other GRP
237 UBCs were identified (Fig 7B-D). Thus, GRP ON UBCs project to other GRP ON UBCs in a feed-forward
238 excitatory circuit that is likely to prolong the duration of an excitatory signal.

239

240 ***Axonal projections from OFF UBCs to other OFF UBCs***

To address whether OFF UBCs project axons to other OFF UBCs, we exploited the observation that the P079 line expresses mCitrine in some, but not all, calretinin-expressing OFF UBCs. Thus, when calretinin is labeled immunohistochemically using a non-green fluorophore, all OFF UBCs are revealed and their brushes can be examined for the presence of connections from mCitrine-labeled P079 OFF UBCs axon terminals. Several examples for OFF to OFF UBC synaptic connections were confirmed anatomically (Fig 8). In some cases, calretinin(+) axon terminals innervated the brushes of P079 UBCs that were also calretinin(+) (Fig 8A-B). In other cases, the P079 UBC terminal contacted calretinin(+) UBCs that were not labeled transgenically in the P079 line (Fig 8C).

Brainbow2.1-Confetti reporter mice were crossed with a line that expresses Cre in calretinin(+) neurons after induction by tamoxifen (Taniguchi et al., 2011). Tamoxifen induced the expression of fluorescent proteins in a subset of these calretinin(+) OFF UBCs and were amplified with antibodies as above (Fig 9A). Several examples are shown, confirming that calretinin(+) OFF UBCs provide input to one another (Fig 9B-D). In one of these examples an axon terminal appeared to contact the soma of a postsynaptic UBC (Fig 9C), which has been previously reported to occur between extrinsic mossy fibers and UBC somata (Balmer and Trussell, 2019). In another case, an axon terminal appeared to project a narrow fiber to the edge of the dendritic brush of a postsynaptic UBC (Fig 9D). These presence of large or small contacts implies differences in synaptic strength, suggesting that OFF UBCs may provide strong synaptic signals to one another (Fig 9B) or presumably weaker signals (Fig 9C-D) that are subsequently integrated with other inputs.

Computational models predict transformations of spiking patterns through synaptically connected ON and OFF UBCs

To address how spiking activity may be transformed by different types of UBCs, computational models were developed to simulate the essential features of ON and OFF UBCs, including their passive electrical properties, synaptic current responses, and spiking patterns. UBCs can fire spontaneously or be silent in acute brain slices (van Dorp and De Zeeuw, 2015; Kim et al., 2012). We chose to make the OFF UBCs spontaneously active in this model so that synaptic input would produce a pause in firing (OFF response) that could be easily measured. By contrast, we made ON UBCs not spontaneously active so that synaptic input would produce a burst of action potentials (ON response). Action potentials triggered glutamate concentration transients that drove the conductance of model AMPA receptors in ON UBCs and mGluR2 in OFF UBCs (see Methods). We contrasted simple cases of an excitatory input to either and ON or OFF UBC, with a more complex case in which the excitatory input drove an "intermediate" UBC which then synapsed on a second UBC. In this way, we could examine the predicted outcomes of ON to ON, ON to OFF, OFF to ON, and OFF to OFF scenarios.

Serial ON UBCs multiply burst duration

Presynaptic input to an ON UBC produced bursts of action potentials that multiplied in duration in a circuit with an intermediate ON UBC (Fig 10A-C). Three presynaptic spikes in a burst lasting 19.6 ms produced a burst of 12 action potentials in the first UBC, lasting 358.0 ms, and 35 action potentials in the second UBC, lasting 1175.3 ms, ~60 times longer than the initial presynaptic input (Fig 10A-B). The

281 enhancement of the spiking duration both in the first and second ON UBC were more pronounced with
282 shorter bursts of presynaptic input and began to plateau at longer durations of input (Fig 10C). The
283 plateau in spiking duration occurs because the rebound AMPA receptor-mediated slow EPSC that occurs
284 at the end of synaptic stimulation in ON UBCs reaches a maximum after ~100 ms of synaptic stimulation
285 (Lu et al., 2017).

286

287 ***Intermediate ON UBCs extend the pause in postsynaptic OFF UBCs***

288 A burst of presynaptic spikes causes a pause in spontaneous firing in OFF UBCs, due to the
289 outward current produced by mGluR2 (Fig 10D). When an intermediate ON UBC was present between
290 the presynaptic axon and the OFF UBC, the synaptic signal to the OFF UBC was extended, and therefore
291 increased the mGluR2 current, markedly lengthening the duration of the pause in spiking (Fig 10E-F).
292 Indeed, the presence of an intermediate ON UBC increased the duration of the pause in the
293 postsynaptic OFF UBC by ~940 ms following 1-10 presynaptic action potentials (indicated by an upward
294 shift in the curve in Fig 10G). The small difference in how much the pause was lengthened across the
295 range of 1-10 presynaptic spikes is due to the intermediate ON UBC's response—even a single
296 presynaptic spike produces a burst of action potentials that is only slightly extended by longer trains of
297 presynaptic input. Across a population of ON UBCs, however, the size and duration of the slow inward
298 currents that drive their firing vary and would thus extend the pause of a postsynaptic OFF UBC for
299 different durations.

300

301 ***Intermediate OFF UBC produce a delayed pause in postsynaptic ON UBC***

302 Because OFF UBCs fired spontaneously in our model, an ON UBC postsynaptic to an
303 intermediate OFF UBC fired with an irregular spiking pattern (Fig 11A). Presynaptic input to the
304 intermediate OFF UBC paused both its firing and its release of glutamate onto the postsynaptic ON UBC,
305 which therefore produced a pause in the postsynaptic ON UBC. However, this pause only occurred after
306 a delay of about 370 ms, due to the slow AMPA receptor mediated EPSC in the ON UBC that decayed
307 slowly until it no longer drove spiking**.** The length of the delay before the pause began is related to the
308 strength of the AMPA receptor-mediated current in the postsynaptic ON UBC. The length of the pause in
309 the ON UBC depends on how long the intermediate OFF UBCs pauses. Thus, an intermediate OFF UBC
310 converts the usual excitatory ON UBC response to a pause that is similar to that of the OFF UBC itself.
311 However, the pause is distinct from that of OFF UBCs, because it is delayed and briefer (Fig 11B).

312

313 ***Serial OFF UBCs produce a delayed burst in postsynaptic OFF UBC***

314 Finally, we considered the case of a connection between two OFF UBCs. In a circuit with a
315 spontaneously firing OFF UBC synapsing onto another OFF UBC (labeled OFF1 and OFF2 respectively, in
316 Fig 11C-D), the tonic glutamatergic input and mGluR2 inhibition prevented spontaneous spiking in the
317 postsynaptic cell. When the intermediate OFF UBC received a burst of presynaptic input, it was inhibited
318 by its own mGluR2 current and therefore stopped firing, thereby disinhibiting the postsynaptic OFF UBC,
319 which then fired after a delay (Fig 11C). Note that this firing would be more pronounced had we

320 incorporated calcium and TRP conductances that contribute to a 'late onset response' in UBCs (Locatelli
321 et al., 2013; Subramaniyam et al., 2014). The duration of the delayed firing in the second postsynaptic
322 OFF UBC depended on the duration of presynaptic input signal to the intermediate UBC (Fig 11D).
323 Moreover, the delay between the last spike in the intermediate OFF UBC and the first spike in the
324 postsynaptic OFF UBC was contingent on the slow decay of the mGluR2 current and was 1082.7 ms in
325 the example in Fig 11C.

326 In summary, our modeling suggests that feed-forward circuits of ON and OFF UBCs transform
327 presynaptic signals by producing an extended spike burst (ON to ON), extended pause (ON to OFF),
328 pause after a delay (OFF to ON), or burst after a delay (OFF to OFF) (Fig 12). This diversification of spiking
329 patterns and durations may be important for maintaining sensory representations of movement and
330 mechanisms of adaptive learning.

331

332 **DISCUSSION**

333 ***GRP and P079 mouse lines label distinct UBC subtypes that form parallel and convergent pathways***

334 Transgenic mice were generated that expressed a green fluorescent protein in OFF UBCs and a
335 red fluorescent protein in ON UBCs in the same tissue. Virtually no neurons expressed both fluorescent
336 proteins. Immunohistochemical analysis showed that all GRP UBCs expressed mGluR1 and most P079
337 UBCs expressed calretinin in both cerebellum and dorsal cochlear nucleus. GRP and P079 UBCs had
338 different average soma sizes and distributions in the cerebellum. Whole-cell recordings in acute brain
339 slices confirmed that the GRP UBCs produce excitatory ON responses mediated by mGluR1 and AMPA
340 receptors, and that P079 UBCs produce inhibitory OFF responses mediated by mGluR2. Their membrane
341 capacitance and excitability were so distinct that the distributions of these properties were almost non-
342 overlapping. These results provide further evidence that some UBC subtypes are genetically and
343 functionally distinct, despite the observation that when the entire population of UBCs is examined, their
344 electrophysiological responses form a continuum from entirely excited by glutamate to entirely inhibited
345 by glutamate (Guo et al., 2021; Kozareva et al., 2021).

346 The UBCs in these mouse lines expressed the fluorescent proteins throughout their axons and
347 presynaptic terminals, which revealed for the first time that axon terminals from one UBC subtype
348 contact the dendric brushes of the other UBC subtype. We also showed that UBCs of the same subtype
349 provide input to one another, by labeling GRP or calretinin-Cre UBCs with different fluorescent proteins
350 using the Brainbow2.1-Confetti reporter line. This result was confirmed with additional approaches that
351 utilized the incomplete labeling of mGluR1(+) ON UBCs in the GRP line and the incomplete labeling of
352 calretinin(+) OFF UBCs in the P079 line. Earlier work reported that that mGluR1(+) UBCs and calretinin(+)
353 UBCs form parallel pathways (Nunzi et al., 2002). Our current data extends the previous result by
354 showing that the even more specific subtypes of GRP or P079 UBCs provide input to members of their
355 own subtype. These networks of UBCs could provide the granule layer with a circuit mechanism to
356 diversify and extend the pattern of spiking produced by mossy fiber input.

357 Anatomically identifiable connections between UBCs were not present in all brain slices and
358 finding them required a careful search. UBC labeling was sparse due to the highly specific genetic
359 labeling techniques and further sparsification by the Brainbow reporter, which made it impossible to

360 estimate the density of these UBC to UBC connections. Electrophysiological evidence suggests that UBC
361 to UBC connections are not common, because spontaneous EPSCs that would indicate a spontaneously
362 firing presynaptic UBC are only rarely observed in UBCs recorded in acute brain slices. In an analysis of
363 feedforward excitation of granule layer neurons, only 4 out of 140 UBCs had this indirect evidence of a
364 firing presynaptic UBC (van Dorp and De Zeeuw, 2015), which suggests that UBC to UBC connections
365 may be rare. On the other hand, previous work using organotypic slice cultures from P8 mice estimated
366 that 2/3 of the UBC population receives input from other UBCs (Nunzi & Mugnaini, 2000). This suggests
367 a much higher density of UBC to UBC connections, but could be due to the young age of the brains used,
368 which is before UBCs have matured (Morin et al., 2001), and also due to increased collateral sprouting
369 that can occur in culture (Jaeger et al., 1988). Another study imaged 2-4 week old rat cerebellar slices at
370 an electron microscopic level and found that 4 out of 14 UBC axon terminals contacted UBC brushes
371 (Diño et al., 2000). Future work is necessary to accurately estimate the density and impact of
372 feedforward UBC circuits.

373 The purpose of this study was to reveal the postsynaptic targets of UBCs with a focus on ON and
374 OFF UBC subtypes. However, it is important to emphasize that the final output and main target of UBCs
375 is granule cells. Most of the labeled UBC axon terminals did not synapse on UBCs and are therefore
376 presumed to synapse on numerous granule cells. Even the axon terminals that targeted UBCs likely also
377 contacted granule cells. Thus, UBCs are interneurons that, when positioned between mossy fibers and
378 granule cells, modify the input to granule cells and have the capacity to synchronize the firing of large
379 ensembles of granule cells via their branching axons and large terminals.

380 The approaches used here were not able to determine the existence of networks of more than 2
381 UBCs connected one after the other. If present, 3 or more UBCs in series could extend and transform the
382 input in even more dramatic ways. The temporal diversity that UBC circuits generate may underlie the
383 flexibility of the cerebellum to coordinate movements over a broad range of behaviors.

384 ***Limitations of the model***

385 Here we addressed how feedforward glutamatergic excitation and inhibition is transformed
386 from one UBC to the next depending on their subtype. The model focuses on AMPA receptor mediated
387 excitation and mGluR2 mediated inhibition. One limitation of the model is that it does not consider
388 feedforward and lateral inhibition from Golgi cells, which shape the spiking of UBCs in response to
389 afferent stimulation. Golgi cells receive mossy fiber input and inhibit UBCs through their corelease of
390 GABA and glycine (Dugue et al., 2005; Rousseau et al., 2012). Golgi cells control the temporal dynamics
391 of the firing of granule cells as well as their gain (Rossi et al., 2003; Kanichay and Silver, 2008) and are
392 critical to larger scale dynamics of the cerebellar cortical network (D'Angelo, 2008). Purkinje cells
393 provide additional inhibition to ON UBCs that could influence how UBC circuits transform signals (Guo et
394 al., 2016). A more complex model that implements Golgi cells and other critical circuit elements will be
395 needed to investigate the role of feedforward UBC circuits in cerebellar network dynamics and motor
396 behaviors in vivo.

397 ***UBC circuits generate a broad range of firing patterns and may be essential for cerebellar learning***

398 Vestibular afferents that encode head movements synapse on both UBCs and granule cells.
399 Granule cells that receive this input are likely to fire in phase with the input signal. A single intermediate
400 UBC would shift the phase of firing of its postsynaptic granule cells, depending on the UBC's response to
401 glutamatergic input, which varies from nearly complete inhibition (e.g. P079 OFF UBC) to complete
402 excitation (e.g. GRP ON UBC) (Guo et al., 2021; Kozareva et al., 2021). For example, an intermediate ON
403 UBC between a presynaptic input and another UBC extended the signal markedly in our models. In
404 circuits with an intermediate OFF UBC, the postsynaptic UBCs signal was inverted: ON UBCs paused
405 when they were no longer driven by glutamate, and OFF UBCs fired when they were no longer inhibited
406 by glutamate. The signal that granule cells subsequently receive would be a burst or pause in firing that
407 lasts for hundreds or thousands of milliseconds. We suggest that these transformations could provide a
408 circuit mechanism for maintaining a sensory representation of movement for seconds, which is thought
409 to be necessary to modulate low-frequency vestibular responses such as compensatory eye movements.

410 The delays introduced by an intermediate UBC were due to the slow decay of the excitatory or
411 inhibitory synaptic currents produced by the presynaptic input. Other cellular and synaptic properties
412 that would shape the timing of pauses, delays, and bursts, include the amount of glutamate released
413 and the rate of its removal, the geometry of the extracellular space, glutamate receptor number and
414 localization, short-term synaptic plasticity, currents underlying rebound spiking, and intrinsic excitability
415 (Kim et al., 2012; Kinney et al., 2013; Locatelli et al., 2013; Zampini et al., 2016; Lu et al., 2017; Balmer et
416 al., 2021). The combination of numerous mechanisms that shape the signal as it is transmitted along the
417 granule layer circuit could produce tunable delay lines essential for sensory representation on an
418 enormous range of time scales.

419 Extending the duration of a sensory feedback signal may also be essential for motor learning
420 when there is a significant delay between the motor output and the sensory feedback, for example,
421 when throwing an object at distant target, a challenge referred to as the credit assignment problem
422 (Sutton and Barto, 1981; Raymond and Lisberger, 1998; Suvrathan, 2019). There are a variety of ways
423 that the cerebellum could extend a signal in time, such as slow axonal conduction, long membrane time
424 constants, inhibition followed by rebound spiking, and slow intracellular processes (Braitenberg, 1967;
425 Rossi et al., 1995; Fiala et al., 1996; Hooper et al., 2002; D'Angelo and De Zeeuw, 2009; van Dorp and De
426 Zeeuw, 2014). UBCs circuits represent another mechanism that could prolong granule cell firing and
427 contribute to the maintenance of sensory signals that underly motor learning in behaviors with delayed
428 sensory feedback.

429 The diversification of spiking patterns by intermediate UBCs may contribute to the pattern
430 separation that is necessary for theories of cerebellar learning (Marr, 1969; Albus, 1971; Ito, 1982;
431 Kennedy et al., 2014; Zampini et al., 2016). In one of the best understood cerebellum-like circuits, the
432 electrosensory lobe of electric fish, UBCs are essential to produce temporally diverse and delayed
433 spiking patterns that are necessary for accurate cancellation of self-generated signals (Kennedy et al.,
434 2014). The authors report that a post-inhibitory rebound that occurred in UBCs may account for the
435 delayed spiking patterns. The presence of synaptic pathways with multiple UBCs could contribute to
436 these long pauses and delays that may be critical for adaptive learning on time scales ranging from
437 hundreds of milliseconds to tens of seconds.

438

439 ***Sources of synaptic input to UBC subtypes***

The firing rates of putative UBCs recorded in vivo in the vestibular cerebellum of mammals follow head velocity and eye movements, in some cases with delays of hundreds of milliseconds (Simpson et al., 2005; Barmack and Yakhnitsa, 2008; Hensbroek et al., 2015). Our data suggests that these long delays could be implemented by feed-forward circuits containing multiple UBCs. It is unknown whether UBCs that are labeled in the GRP or P079 mouse lines are a subtype that receives a specific source of input. In lobe X, ON UBCs defined by their electrophysiological response or mGluR1-expression receive input from both primary vestibular afferents and second-order mossy fibers from the vestibular nucleus, while OFF UBCs only receive vestibular nuclear input (Balmer and Trussell, 2019). Understanding whether the UBCs labeled in these mouse lines receive head or eye movement signals, integrated signals that encode head orientation relative to gravity, or another type of signal, would help elucidate their specific roles in cerebellar functions.

METHODS

Animals

Mice of both sexes were used from the following mouse lines and their crosses: P079 line: Et(tTA/mCitrine)P079Sbn (Shima et al., 2016), GRP-Cre line: Tg(Grp-Cre)KH107Gsat (Gerfen et al., 2013), Ai9 line: Gt(ROSA)$^{26Sortm9(CAG\text{-}tdTomato)Hze}$ (Madisen et al., 2010), Brainbow2.1-Confetti line: Gt(ROSA)26Sortm1$^{(CAG\text{-}Brainbow2.1)Cle/J}$ (Snippert et al., 2010), calretinin-Cre line: Calb2$^{tm2.1(cre/ERT2)Zjh/J}$ (Taniguchi et al., 2011). Cre-mediated recombination was induced in calretinin-Cre mice by intraperitoneal injections of 10 mg/ml tamoxifen (Sigma T5648) in corn oil at a dose of 75 mg/kg per day for 2-3 days and perfused 2-3 weeks later. Mice were bred in a colony maintained in the animal facility managed by the Department of Animal Care and Technologies and all procedures were approved by Arizona State University's Institutional Animal Care and Use Committee. Transgenic mice were genotyped by light at P0-P3 or by PCR.

Brain slice preparation

For acute brain slice electrophysiology, male and female P079 and GRP-Cre/Ai9 mice were used at ages P21-35. Animals were deeply anesthetized with isoflurane and the brain was extracted under ice-cold high-sucrose artificial cerebral spinal fluid (ACSF) containing the following (in mM): 87 NaCl, 75 sucrose, 25 $NaHCO_3$, 25 glucose, 2.5 KCl, 1.25 NaH_2PO_4, 0.4 Na-ascorbate, 2 Na-pyruvate, 0.5 $CaCl_2$, 7 $MgCl_2$, bubbled with 5% CO_2/95% O_2. Parasagittal cerebellum sections 200-300 µm thick were cut with a vibratome (7000smz-2, Campden Instruments) in ice-cold high-sucrose ACSF. Slices recovered at 35°C for 30-40 minutes, in ACSF containing the following (in mM): 130 NaCl, 2.1 KCl, 1.2 KH_2PO_4, 3 Na-HEPES, 10 glucose, 20 $NaHCO_3$, 0.4 Na-ascorbate, 2 Na-pyruvate, 1.5 $CaCl_2$, 1 $MgSO_4$, bubbled with 5% CO_2/95% O_2 (300–305 mOsm). Slices were maintained at room temperature (~23°C) until recording. Recordings were performed from lobe X of the cerebellum within 6 hours of preparation.

Electrophysiological recordings

Acute brain slices were perfused with ACSF using a peristaltic pump (Ismatec) at 2-3 ml/min, and maintained at 32-34°C with an inline heater (Warner Instruments). ACSF contained 0.5 µM Strychnine

480 and 5 µM SR95531 to block synaptic inhibition. The recording set up was composed of an Olympus BX51
481 fixed-stage microscope with Dodt gradient contrast optics (Dodt et al., 2002), and 4X and 60X (water
482 immersion) Olympus objectives. UBCs were initially identified by soma size or transgenic fluorescence
483 and confirmed by intracellular filling with 5 µM Alexa Fluor 568 or 488 hydrazide sodium salt (Life
484 Technologies). Patch electrodes were pulled with borosilicate glass capillaries (OD 1.2 mm and ID 0.68
485 mm, AM Systems) with a horizontal puller (P1000, Sutter Instruments). Intracellular recording solution
486 contained (mM): 113 K-gluconate, 9 HEPES, 4.5 $MgCl_2$, 0.1 EGTA, 14 Tris-phosphocreatine, 4 Na_2-ATP,
487 0.3 tris-GTP, 0.1-0.3% biocytin, 290 mOsm, pH 7.2-7.25. All recordings were corrected for a -10 mV
488 junction potential. Data were acquired using a Multiclamp 700B amplifier and pClamp 11 software
489 (Molecular Devices). Signals were acquired with 5-10X gain, sampled at 50-100 kHz using a Digidata
490 (1550A, Molecular Devices) analog-digital converter, and low-pass filtered at 10 kHz, with further
491 filtering applied offline. Patch pipettes tip resistance was 5-8 MΩ; series resistance was compensated
492 with correction 20-40% and prediction 50-70%, bandwidth 2 kHz. Membrane potential was held
493 constant at -70 mV in voltage clamp experiments. Electrical stimulation was performed using a
494 concentric bipolar electrode (CBBPC75, FHC) placed in the white matter of the sagittal cerebellar slice.
495 Stimuli were evoked using a stimulus isolation unit (Iso-Flex, A.M.P.I.) delivering 100-250 µs duration
496 pulses of 0-90 V.
497

498 *Immunohistochemistry and imaging*
499 Mice were overdosed with isoflurane and perfused through the heart with 0.01 M phosphate buffered
500 saline, 7.4 pH (PBS) followed by 4% paraformaldehyde in PBS. Brains were extracted from the skull and
501 incubated in 4% paraformaldehyde in PBS overnight at 4˚C. 50 µm thick sections were made on a
502 vibratome (7000smz-2, Campden Instruments). To recover cells that were filled with biocytin during
503 whole-cell recording, acute brain slices were fixed 1-2 h in 4% paraformaldehyde in PBS, followed by
504 storage in PBS. Both floating 50 µm sections and 200-300 µm thick acute slices were treated with the
505 following procedures. Sections were rinsed 3 x 5 min in PBS, blocked and permeabilized in 5% BSA, 2%
506 fish gelatin, 0.2% Triton X-100 in PBS for >1 hr at room temperature. Sections were incubated in primary
507 antibodies overnight in 1% fish gelatin in PBS at 4˚C on an orbital shaker. Primary antibodies included
508 chicken polyclonal anti-GFP (1:2000, Aves Labs, GFP-1020, AB_10000240), goat polyclonal anti-mCherry
509 (1:2000, Sicgen, AB0040, AB_2333093), mouse monoclonal anti-rat mGluR1a (1:800, BD Pharmingen,
510 556389, AB_396404), rabbit polyclonal anti-calretinin (1:2000, Swant, 7697, AB_10000342). Sections
511 were rinsed 3 x 5 min in PBS, followed by secondary antibodies (1:500) and streptavidin (1:2000) that
512 were diluted in 1% fish gelatin in PBS and incubated overnight at 4˚C on an orbital shaker. Secondary
513 antibodies included donkey anti-chicken Alexa Fluor 488 (Jackson ImmunoResearch, 715-545-155,
514 AB_2340375), donkey anti-mouse Alexa Fluor 647 (Jackson ImmunoResearch, 715-605-151,
515 AB_2340863), donkey anti-rabbit Alexa Fluor 647 (Jackson ImmunoResearch, 711-605-152,
516 AB_2492288), donkey anti-rabbit Cy3 (Jackson ImmunoResearch, 711-165-152, AB_2307443), donkey
517 ant-goat Cy3 (Jackson ImmunoResearch, 705-165-147, AB_2307351), streptavidin-Alexa Fluor 647
518 (ThermoFisher Scientific, S21374, AB_2336066). Sections were mounted on microscope slides
519 (Superfrost Plus, Fisher Scientific) and coverslipped with Fluoromount-G (Southern Biotech). Images
520 were acquired a confocal microscope (LSM800, Zeiss) with the Airyscan system that reconstructs super-

521 resolution images from a series of images acquired under spatially structured illumination. Images are
522 single optical planes unless otherwise specified.
523

524 *Image quantification*

525 Sagittal brain slices containing lobe X were imaged systematically across the medial-lateral axis. One
526 area in the dorsal region and one area in the ventral region of lobe X in each selected slice was imaged
527 using a 63x objective. The volume was 202.8 µm x 202.8 µm x 10.8 µm for each image using ~12 z-
528 planes. Images were annotated for transgenic expression of tdTomato or mCitrine as well as mGluR1 or
529 calretinin labeling. tdTomato, mCitrine and calretinin labeling is cytoplasmic and UBCs were easily
530 counted if they had a labeled soma and attached dendritic brush. mGluR1 is mostly expressed in the
531 dendrite, but labeling is also present in the soma membrane, which can be observed as a circle. mGluR1
532 UBCs were counted if there was labeling in the dendritic brush that was attached to an apparent
533 mGluR1-labeled soma. This necessarily conservative method of identifying mGluR1-labeled UBCs likely
534 resulted in an underestimation of the total number of mGluR1(+) UBCs.

535 The labeling intensity of mCitrine in P079 UBCs that were mGluR1(+) was compared to P079 UBCs that
536 were mGluR1(-) by measuring the mean pixel intensity in the somas of each type of UBCs. At least one of
537 each type was measured in the same image and same z-plane to account for differences in brightness
538 that could be due to differences in immunohistochemical labeling, image acquisition settings, and depth
539 in the slice (deeper cells are less well labeled due to more limited antibody penetration). For each z-
540 plane with at least one mGluR1(+) and one mGluR1(-) P079 UBC, a difference in brightness was
541 calculated and reported as a relative brightness of the mGluR1(+) P079 UBCs to the brighter mGluR1(-)
542 P079 UBCs.

543

544 *Computational modeling*

545 Single compartment models of ON and OFF UBCs were built using NEURON (Hines and Carnevale, 1997;
546 Carnevale and Hines, 2006) and utilized fast voltage-gated sodium (g_{Na}) and potassium (g_K) conductances
547 to produce action potentials (Destexhe et al., 1994), a slow voltage-gated potassium conductance from
548 a model of cerebellar granule cells ($g_{K\text{-}slow}$) (D'Angelo et al., 2001), and a passive leak conductance (g_{pas}).
549 A hyperpolarization-activated non-specific conductance (g_H) (Kim et al., 2012; Subramaniyam et al.,
550 2014), which was added to ON and OFF UBCs a voltage sag in response to hyperpolarizing current pulses
551 that reproduced those reported in Figure 1 Input resistance of the cells was measured using a -5 pA
552 current pulse and adjusted to approximate GRP ON UBCs and P079 OFF UBCs by adjusting the passive
553 leak conductance. Capacitance was measured from the membrane time constant and adjusted by
554 changing the membrane area. Specific membrane capacitance was set to 1 µF/cm^2. Tables 1-2 shows the
555 variables used in ON and OFF UBCs.

556 Synaptic transmission was implemented by applying glutamate transients simulated with a 3-
557 dimensional diffusion equation to an AMPA receptor model that was fit to ON UBC data (Lu et al., 2017)
558 and described in detail in our previous work (Balmer et al., 2021) (Table 3-4). OFF UBCs have mGluR2
559 receptors that are thought to be distant from the presynaptic release sites (Jaarsma et al., 1998), which
560 we approximated by reducing the amount of glutamate released by a factor of 10 and increasing the

561 distance by 1 µm in the diffusion equation (Table 3). To model mGluR2 currents in P079 UBCs that are
562 mediated by G-protein coupled inwardly rectifying potassium channels, a GABA-B receptor model
563 (Destexhe et al., 1998) was modified to approximate the kinetics of our recorded currents by increasing
564 the unbinding rate from 0.02 ms^{-1} to 0.0215 ms^{-1} (Table 4). A train of 10 presynaptic release events
565 produced an 865 ms long burst in the ON UBC model and a 1545 ms pause in the OFF UBC model, which
566 is within the range observed in our data set.

567

568 **Table 1- ON UBC conductances**

ON UBC		
Modeled conductance	*gmax (S/cm^2)*	*Erev (mV)*
g_{Na}	0.1	50
g_K	0.03	-90
g_H	1e-5	-30
g_{pas}	2e-4	-65
$g_{K\text{-}slow}$	8e-4	-90
Diameter	20 µm	

569

570 **Table 2- OFF UBC conductances**

OFF UBC		
Modeled conductance	*gmax (S/cm^2)*	*Erev (mV)*
g_{Na}	0.1	50
g_K	0.03	-90
g_H	3.1e-4	-30
g_{pas}	7e-5	-62
$g_{K\text{-}slow}$	8e-4	-90
Diameter	27 µm	

571

572

573 **Table 3- Glutamate diffusion at AMPA and mGluR2 receptors**

Glutamate diffusion parameter	*AMPA synapse*	*mGluR2 synapse*
Molecules released (#)	3e6	3e5
Distance (nm)	750	1750
Diffusion coefficient (cm^2/s)	0.33	0.33
Tortuosity	1.55	1.55
Volume fraction	0.21	0.21
Ambient glutamate (mM)	0.005	0

574

575 **Table 4- Synaptic conductances**

Synaptic receptor	*gmax (S/cm^2)*	*Erev (mV)*
ON UBC- AMPA	4e-9	0
OFF UBC- mGluR2	1e-8	-90

576

577 **Conflict of interest statement:** The authors declare no competing financial interests.

578 **Acknowledgements:** Funding was provided by the NIH/NIDCD R00 DC016905, Hearing Health
579 Foundation, and National Ataxia Foundation. We thank Dr. Jason Newbern for confocal microscope use,
580 Dr. Sacha Nelson for the P079 mouse line, and Dr. Larry Trussell for comments on the manuscript.

581

582 **References**

583 Albus JS (1971) A theory of cerebellar function. Math Biosci 10:25–61.
584 Balmer TS, Borges-Merjane C, Trussell LO (2021) Incomplete removal of extracellular glutamate controls
585 synaptic transmission and integration at a cerebellar synapse. eLife 10:e63819.
586 Balmer TS, Trussell LO (2019) Selective targeting of unipolar brush cell subtypes by cerebellar mossy
587 fibers. eLife 8:e44964.
588 Balmer TS, Trussell LO (2021) Trigeminal Contributions to the Dorsal Cochlear Nucleus in Mouse. Front
589 Neurosci 15.
590 Balmer TS, Trussell LO (2022) Descending Axonal Projections from the Inferior Colliculus Target Nearly
591 All Excitatory and Inhibitory Cell Types of the Dorsal Cochlear Nucleus. J Neurosci 42:3381–3393.
592 Barmack NH, Yakhnitsa V (2008) Functions of interneurons in mouse cerebellum. J Neurosci 28:1140–
593 1152.
594 Berthie B, Axelrad H (1994) Granular layer collaterals of the unipolar brush cell axon display rosette-like
595 excrescences. A Golgi study in the rat cerebellar cortex. Neurosci Lett 167:161–165.
596 Borges-Merjane C, Trussell LO (2015) ON and OFF unipolar brush cells transform multisensory inputs to
597 the auditory system. Neuron 85:1029–1042.
598 Braitenberg V (1967) Is the cerebellar cortex a biological clock in the millisecond range? Prog Brain Res
599 25:334–346.
600 Carnevale NT, Hines ML (2006) The NEURON book. Cambridge University Press.
601 D'Angelo E, De Zeeuw CI (2009) Timing and plasticity in the cerebellum: focus on the granular layer.
602 Trends Neurosci 32:30–40.
603 D'Angelo E, Nieus T, Maffei A, Armano S, Rossi P, Taglietti V, Fontana A, Naldi G (2001) Theta-Frequency
604 Bursting and Resonance in Cerebellar Granule Cells: Experimental Evidence and Modeling of a
605 Slow K+-Dependent Mechanism. J Neurosci 21:759–770.
606 D'Angelo E (2008) The critical role of Golgi cells in regulating spatio-temporal integration and plasticity
607 at the cerebellum input stage. Front Neurosci 2 Available at:
608 https://www.frontiersin.org/articles/10.3389/neuro.01.008.2008 [Accessed October 27, 2023].
609 Destexhe A, Contreras D, Sejnowski TJ, Steriade M (1994) A model of spindle rhythmicity in the isolated
610 thalamic reticular nucleus. J Neurophysiol 72:803–818.
611 Destexhe A, Mainen ZF, Sejnowski TJ (1998) Kinetic models of synaptic transmission. Methods Neuronal
612 Model 2:1–25.

613 Diño MR, Schuerger RJ, Liu Y-B, Slater NT, Mugnaini E (2000) Unipolar brush cell: a potential feedforward
614 excitatory interneuron of the cerebellum. Neuroscience 98:625–636.
615 Dugue GP, Dumoulin A, Triller A, Dieudonne S (2005) Target-dependent use of co-released inhibitory
616 transmitters at central synapses. J Neurosci 25:6490–6498
617 Fernandez C, Goldberg JM (1971) Physiology of peripheral neurons innervating semicircular canals of the
618 squirrel monkey. II. Response to sinusoidal stimulation and dynamics of peripheral vestibular
619 system. J Neurophysiol 34:661–675.
620 Fiala JC, Grossberg S, Bullock D (1996) Metabotropic Glutamate Receptor Activation in Cerebellar
621 Purkinje Cells as Substrate for Adaptive Timing of the Classically Conditioned Eye-Blink
622 Response. J Neurosci 16:3760–3774.
623 Gerfen CR, Paletzki R, Heintz N (2013) GENSAT BAC cre-recombinase driver lines to study the functional
624 organization of cerebral cortical and basal ganglia circuits. Neuron 80:1368–1383.
625 Guo C, Huson V, Macosko EZ, Regehr WG (2021) Graded heterogeneity of metabotropic signaling
626 underlies a continuum of cell-intrinsic temporal responses in unipolar brush cells. Nat Commun
627 12:5491.
628 Guo C, Witter L, Rudolph S, Elliott HL, Ennis KA, Regehr WG (2016) Purkinje Cells Directly Inhibit Granule
629 Cells in Specialized Regions of the Cerebellar Cortex. Neuron 91:1330–1341.
630 Hensbroek RA, Ruigrok TJ, van Beugen BJ, Maruta J, Simpson JI (2015) Visuo-Vestibular Information
631 Processing by Unipolar Brush Cells in the Rabbit Flocculus. Cerebellum 14:578–583.
632 Hines ML, Carnevale NT (1997) The NEURON simulation environment. Neural Comput 9:1179–1209.
633 Hooper SL, Buchman E, Hobbs KH (2002) A computational role for slow conductances: single-neuron
634 models that measure duration. Nat Neurosci 5:552–556.
635 Ito M (1982) Cerebellar control of the vestibulo-ocular reflex--around the flocculus hypothesis. Annu Rev
636 Neurosci 5:275–296.
637 Jaarsma D, Dino MR, Ohishi H, Shigemoto R, Mugnaini E (1998) Metabotropic glutamate receptors are
638 associated with non-synaptic appendages of unipolar brush cells in rat cerebellar cortex and
639 cochlear nuclear complex. J Neurocytol 27:303–327.
640 Jaeger CB, Kapoor R, Llinás R (1988) Cytology and organization of rat cerebellar organ cultures.
641 Neuroscience 26:509–538.
642 Kanichay RT, Silver RA (2008) Synaptic and Cellular Properties of the Feedforward Inhibitory Circuit
643 within the Input Layer of the Cerebellar Cortex. J Neurosci 28:8955–8967.
644 Kennedy A, Wayne G, Kaifosh P, Alvina K, Abbott LF, Sawtell NB (2014) A temporal basis for predicting
645 the sensory consequences of motor commands in an electric fish. Nat Neurosci 17:416–422.
646 Kim JA, Sekerkova G, Mugnaini E, Martina M (2012) Electrophysiological, morphological, and topological
647 properties of two histochemically distinct subpopulations of cerebellar unipolar brush cells.
648 Cerebellum 11:1012–1025.
649 Kinney JP, Spacek J, Bartol TM, Bajaj CL, Harris KM, Sejnowski TJ (2013) Extracellular sheets and tunnels
650 modulate glutamate diffusion in hippocampal neuropil. J Comp Neurol 521:448–464.
651 Kozareva V, Martin C, Osorno T, Rudolph S, Guo C, Vanderburg C, Nadaf N, Regev A, Regehr WG,
652 Macosko E (2021) A transcriptomic atlas of mouse cerebellar cortex comprehensively defines
653 cell types. Nature 598:214–219.
654 Livet J, Weissman TA, Kang H, Draft RW, Lu J, Bennis RA, Sanes JR, Lichtman JW (2007) Transgenic
655 strategies for combinatorial expression of fluorescent proteins in the nervous system. Nature
656 450:56–62.
657 Locatelli F, Botta L, Prestori F, Masetto S, D'Angelo E (2013) Late-onset bursts evoked by mossy fibre
658 bundle stimulation in unipolar brush cells: evidence for the involvement of H- and TRP-currents.
659 J Physiol 591:899–918.

660 Lu HW, Balmer TS, Romero GE, Trussell LO (2017) Slow AMPAR Synaptic Transmission Is Determined by
661 Stargazin and Glutamate Transporters. Neuron 96:73-80 e4.
662 Madisen L, Zwingman TA, Sunkin SM, Oh SW, Zariwala HA, Gu H, Ng LL, Palmiter RD, Hawrylycz MJ,
663 Jones AR, Lein ES, Zeng H (2010) A robust and high-throughput Cre reporting and
664 characterization system for the whole mouse brain. Nat Neurosci 13:133–140.
665 Marr D (1969) A theory of cerebellar cortex. J Physiol 202:437–470.
666 Morin F, Diño MR, Mugnaini E (2001) Postnatal differentiation of unipolar brush cells and mossy fiber-
667 unipolar brush cell synapses in rat cerebellum. Neuroscience 104:1127–1139.
668 Mugnaini E, Floris A, Wright-Goss M (1994) Extraordinary synapses of the unipolar brush cell: an
669 electron microscopic study in the rat cerebellum. Synapse 16:284–311.
670 Mugnaini E, Sekerkova G, Martina M (2011) The unipolar brush cell: a remarkable neuron finally
671 receiving deserved attention. Brain Res Rev 66:220–245.
672 Nunzi MG, Birnstiel S, Bhattacharyya BJ, Slater NT, Mugnaini E (2001) Unipolar brush cells form a
673 glutamatergic projection system within the mouse cerebellar cortex. J Comp Neurol 434:329–
674 341.
675 Nunzi M-G, Mugnaini E (2000) Unipolar brush cell axons form a large system of intrinsic mossy fibers in
676 the postnatal vestibulocerebellum. J Comp Neurol 422:55–65.
677 Nunzi MG, Russo M, Mugnaini E (2003) Vesicular glutamate transporters VGLUT1 and VGLUT2 define
678 two subsets of unipolar brush cells in organotypic cultures of mouse vestibulocerebellum.
679 Neuroscience 122:359–371.
680 Nunzi MG, Shigemoto R, Mugnaini E (2002) Differential expression of calretinin and metabotropic
681 glutamate receptor mGluR1alpha defines subsets of unipolar brush cells in mouse cerebellum. J
682 Comp Neurol 451:189–199.
683 Raphan Th, Matsuo V, Cohen B (1979) Velocity storage in the vestibulo-ocular reflex arc (VOR). Exp Brain
684 Res 35:229–248.
685 Raymond JL, Lisberger SG (1998) Neural learning rules for the vestibulo-ocular reflex. J Neurosci
686 18:9112–9129.
687 Rossi DJ, Alford S, Mugnaini E, Slater NT (1995) Properties of transmission at a giant glutamatergic
688 synapse in cerebellum: the mossy fiber-unipolar brush cell synapse. J Neurophysiol 74:24–42.
689 Rossi DJ, Hamann M, Attwell D (2003) Multiple modes of GABAergic inhibition of rat cerebellar granule
690 cells. J Physiol 548:97–110.
691 Rousseau CV, Dugue GP, Dumoulin A, Mugnaini E, Dieudonne S, Diana MA (2012) Mixed inhibitory
692 synaptic balance correlates with glutamatergic synaptic phenotype in cerebellar unipolar brush
693 cells. J Neurosci 32:4632–4644.
694 Ryugo DK, Haenggeli CA, Doucet JR (2003) Multimodal inputs to the granule cell domain of the cochlear
695 nucleus. Exp Brain Res 153:477–485.
696 Sekerkova G, Watanabe M, Martina M, Mugnaini E (2014) Differential distribution of phospholipase C
697 beta isoforms and diaglycerol kinase-beta in rodents cerebella corroborates the division of
698 unipolar brush cells into two major subtypes. Brain Struct Funct 219:719–749.
699 Shima Y, Sugino K, Hempel CM, Shima M, Taneja P, Bullis JB, Mehta S, Lois C, Nelson SB (2016) A
700 Mammalian enhancer trap resource for discovering and manipulating neuronal cell types. Elife
701 5:e13503.
702 Simpson JI, Hulscher HC, Sabel-Goedknegt E, Ruigrok TJ (2005) Between in and out: linking morphology
703 and physiology of cerebellar cortical interneurons. Prog Brain Res 148:329–340.
704 Snippert HJ, van der Flier LG, Sato T, van Es JH, van den Born M, Kroon-Veenboer C, Barker N, Klein AM,
705 van Rheenen J, Simons BD, Clevers H (2010) Intestinal crypt homeostasis results from neutral
706 competition between symmetrically dividing Lgr5 stem cells. Cell 143:134–144.

Subramaniyam S, Solinas S, Perin P, Locatelli F, Masetto S, D'Angelo E (2014) Computational modeling predicts the ionic mechanism of late-onset responses in unipolar brush cells. Front Cell Neurosci 8:237.

Sutton RS, Barto AG (1981) Toward a modern theory of adaptive networks: expectation and prediction. Psychol Rev 88:135–170.

Suvrathan A (2019) Beyond STDP—towards diverse and functionally relevant plasticity rules. Curr Opin Neurobiol 54:12–19.

Taniguchi H, He M, Wu P, Kim S, Paik R, Sugino K, Kvitsiani D, Fu Y, Lu J, Lin Y, Miyoshi G, Shima Y, Fishell G, Nelson SB, Huang ZJ (2011) A resource of Cre driver lines for genetic targeting of GABAergic neurons in cerebral cortex. Neuron 71:995–1013.

van Dorp S, De Zeeuw CI (2014) Variable timing of synaptic transmission in cerebellar unipolar brush cells. Proc Natl Acad Sci U S A 111:5403–5408.

van Dorp S, De Zeeuw CI (2015) Forward signaling by unipolar brush cells in the mouse cerebellum. Cerebellum 14:528–533.

Yakushin SB, Raphan T, Cohen B (2017) Coding of Velocity Storage in the Vestibular Nuclei. Front Neurol 8.

Zampini V, Liu JK, Diana MA, Maldonado PP, Brunel N, Dieudonne S (2016) Mechanisms and functional roles of glutamatergic synapse diversity in a cerebellar circuit. eLife 5.

FIGURES

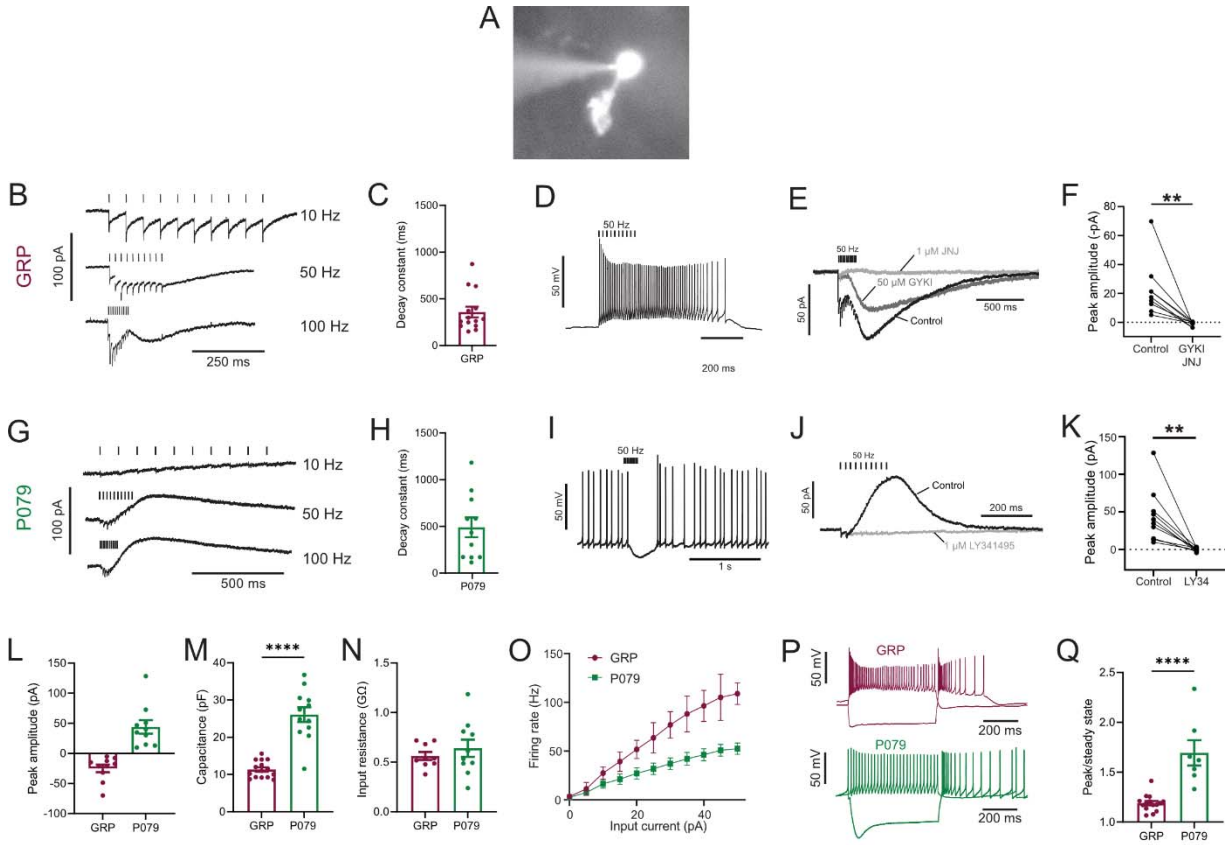

Figure 1- Physiological characterization of GRP and P079 UBCs in acute brain slices

A) Representative image of UBC in whole cell patch clamp recording filled with Alexa Fluor 488.
B) In GRP UBCs, mossy fiber stimulation evoked fast excitatory post synaptic currents and a slow inward current that became more prominent with faster stimulation rates.
C) Summary of the decay constants of the slow EPSCs generated by a train of 10 stimuli at a 50 Hz rate in GRP UBCs.
D) In current clamp, 50 Hz stimulation produced a burst of spikes that outlasted the stimulus.
E) The fast EPSCs and part of the slow EPSC was blocked by an AMPA receptor antagonist (50 µM GYKI53655). The remaining slow EPSC was blocked by an mGluR1 antagonist (1 µM JNJ16259685).
F) Inward currents in GRP UBCs were consistently blocked by AMPA receptor and mGluR1 receptor antagonists.
G) In P079 UBCs, mossy fiber stimulation evoked slow outward currents.
H) Summary of the decay constants of the slow outward currents generated by a train of 10 stimuli at a 50Hz rate in P079 UBCs.
I) In current clamp, 50 Hz stimulation generated a pause in spontaneous action potential firing in P079 UBCs.
J) The outward current was blocked by an mGluR2 antagonist (1 µM LY341495).
K) Outward currents in P079 UBCs were entirely blocked by 1 µM LY341495.
L) Peak amplitudes of the slow currents were inward in all recorded GRP UBCs and outward in all recorded P079 UBCs.
M) The capacitance was significantly higher in P079 UBCs compared to GRP UBCs.
N) The input resistance was not different between GRP UBCs and P079 UBCs.

O) Frequency-intensity curves show that GRP UBCs are more excitable and are able to fire at faster rates than P079 UBCs.

P) Example traces showing the response of GRP and P079 UBCs to 40-pA depolarizing and -100-pA hyperpolarizing 500 ms current steps. The GRP UBCs fire at a higher rate than P079 UBCs during a 40-pA depolarizing current step. The P079 UBCs have a more prominent voltage sag in response to the -100-pA hyperpolarizing current step than the GRP UBCs.

Q) The sag ratio was larger in P079 UBCs than GRP UBCs.

Stimulation artifacts have been removed for clarity. Error bars are SEM.

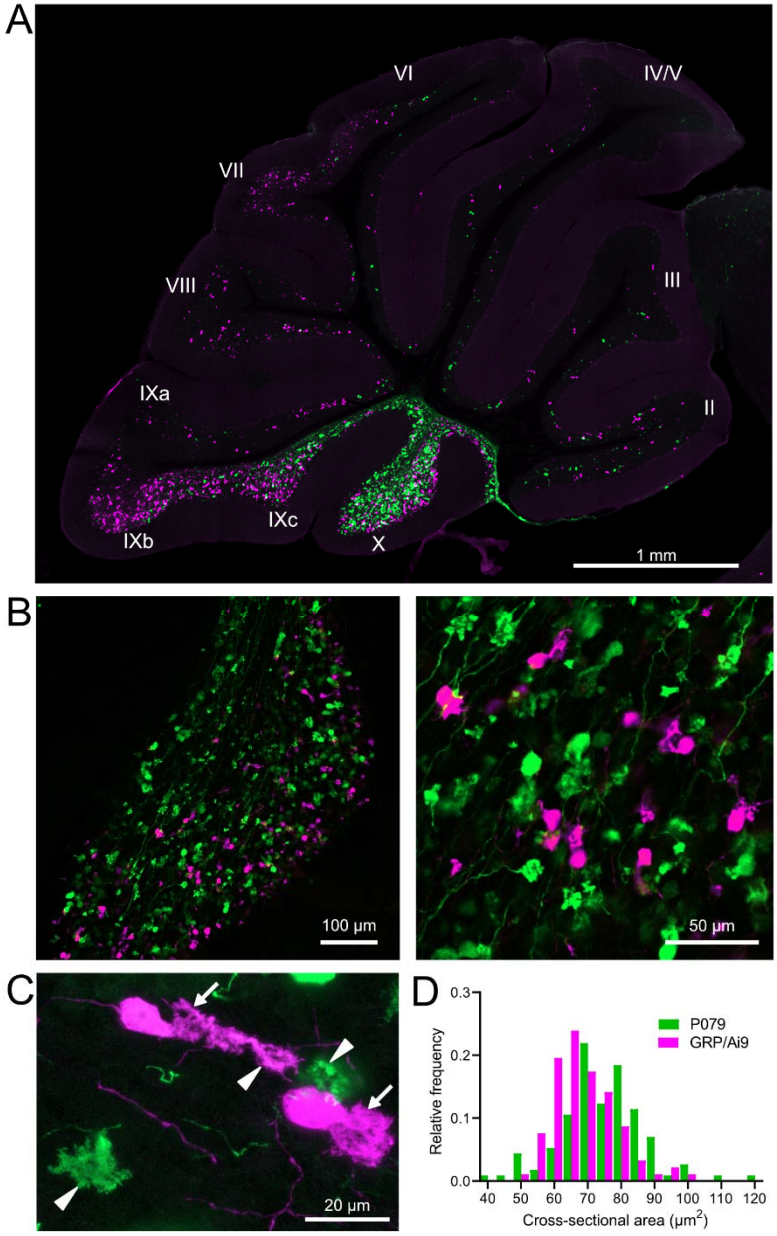

Figure 2- GRP/Ai9/P079 mouse line labels two distinct subsets of UBCs

A) Sagittal section of cerebellar vermis. Fluorescence is restricted to UBC cell types. P079 UBCs (mCitrine- green) are present in high density in lobe X and lobe IXc, while GRP UBCs (tdTomato- magenta) are present in those lobes as well as lobe IXb and in a lower density in Lobe VI-VIII. Maximum intensity projection.

764 B) Left- Sagittal section showing expression of mCitrine labeling P079 UBCs and tdTomato labeling GRP UBCs in
765 lobe X. More GRP UBCs are present in the dorsal leaflet than the ventral leaflet. Right- UBCs and their axons and
766 terminals are well labeled. Only rarely were UBCs labeled with both colors. Maximum intensity projection.
767 C) Magnified view of UBCs with their dendritic brushes indicated with arrows. Two P079 terminals and one GRP
768 terminal are indicated with arrowheads. The GRP UBC at the top of the image demonstrates the challenge of
769 differentiating the dendritic brush of a UBC from a terminal that is labeled with the same fluorophore. Maximum
770 intensity projection.
771 D) In lobe X, P079 UBCs had larger somas than GRP UBCs, although there is a somewhat bimodal distribution in the
772 P079 population.
773

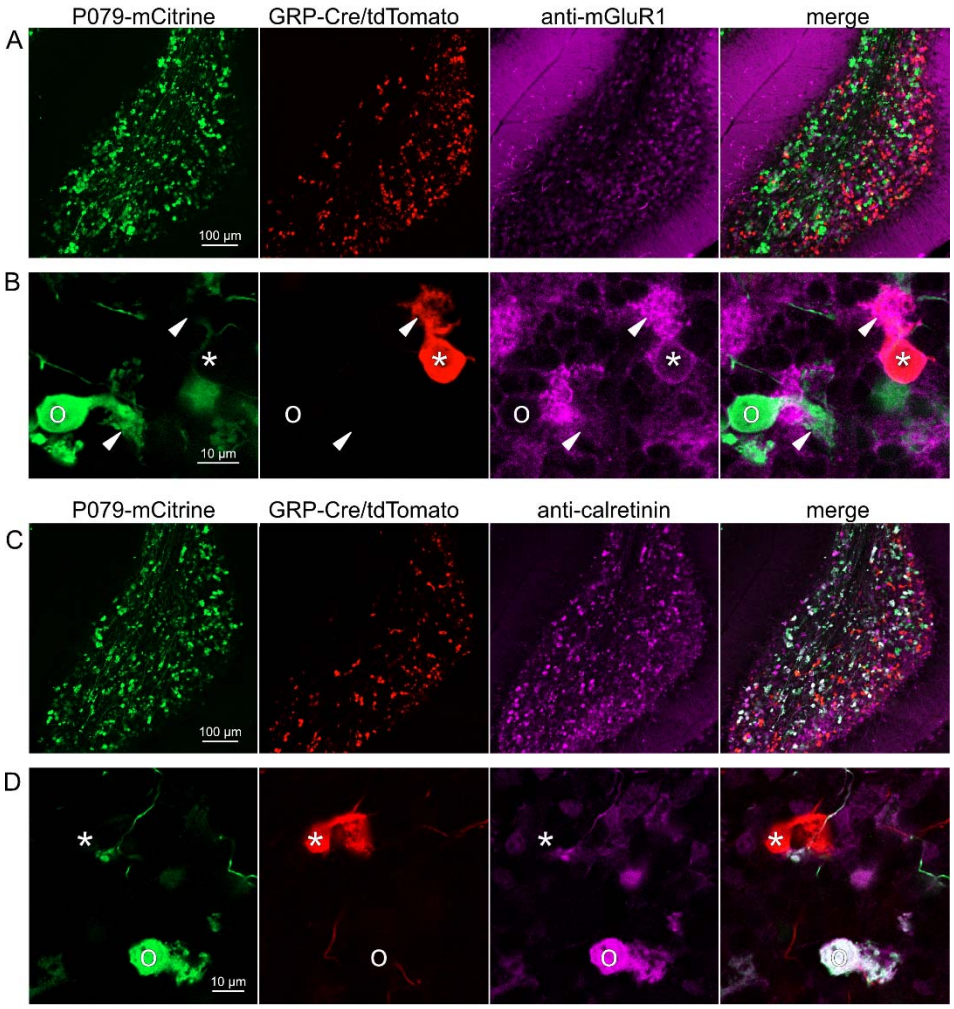

774

775 *Figure 3- Expression of mGluR1 and calretinin in GRP and P079 UBCs in the cerebellum*
776 A) Sagittal section of lobe X showing genetically expressed mCitrine (green) from the P079 mouse, tdTomato (red)
777 from the GRP-Cre/Ai9 mouse, and immunohistochemical labeling of mGluR1 (magenta). Maximum intensity
778 projections.
779 B) Example of a P079 UBC (soma indicated with O, brush indicated with arrowhead), GRP UBC (soma indicated with
780 *, brush indicated with arrowhead). The GRP UBCs expresses mGluR1 in the somatic membrane and dendritic
781 brush. Most P079 UBCs do not express mGluR1. Single image planes.

782 C) Sagittal section of lobe X showing genetically expressed mCitrine (green) from the P079 mouse, tdTomato (red)
783 from the GRP-Cre/Ai9 mouse, and immunohistochemical labeling of calretinin (magenta). Maximum intensity
784 projections.
785 D) Example of a P079 UBC (soma indicated with O), GRP UBC (soma indicated with *). The P079 UBCs express
786 calretinin in their cytoplasm. GRP UBCs do not express calretinin.
787

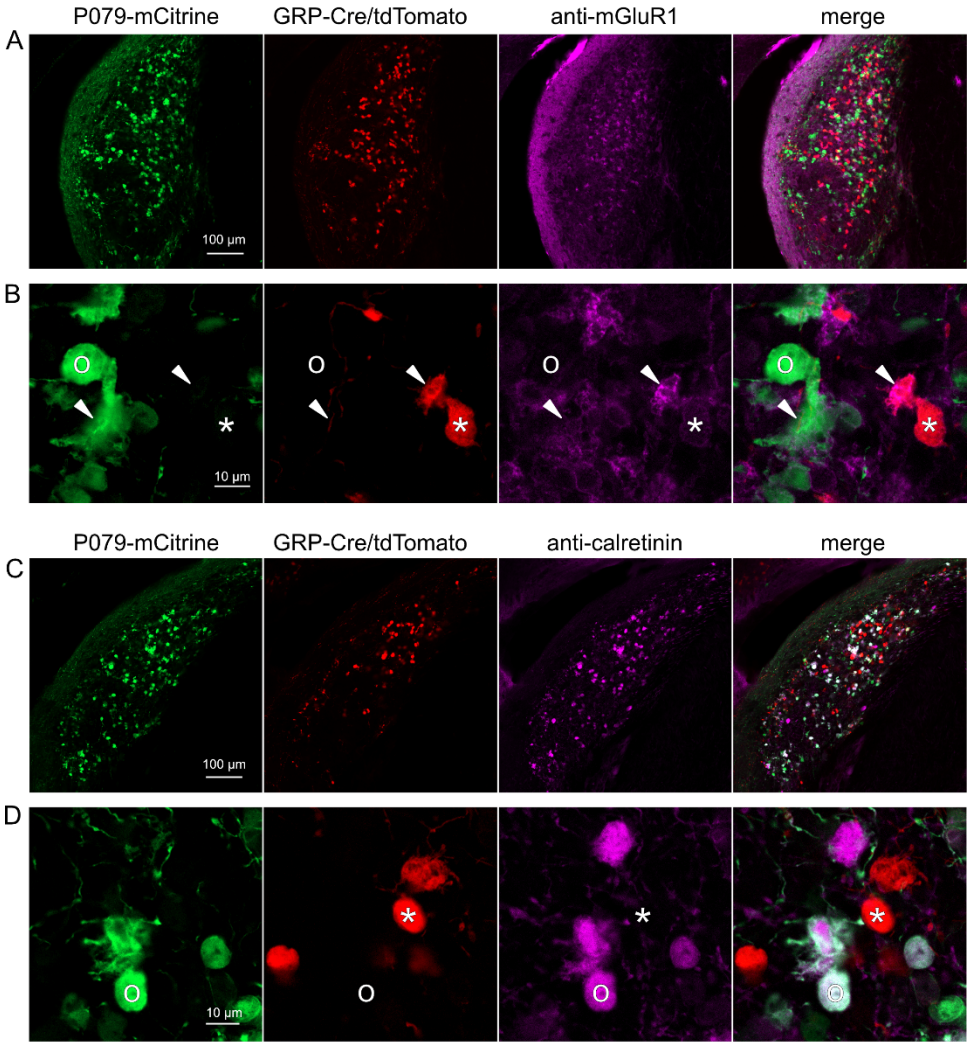

788

789 *Figure 4- Expression of mGluR1 and calretinin in P079 and GRP UBCs in the dorsal cochlear nucleus*
790 A) Coronal section of the dorsal cochlear nucleus showing genetically expressed mCitrine (green) from the P079
791 allele, tdTomato (red) from the GRP-Cre/Ai9 alleles, and immunohistochemical labeling of mGluR1 (magenta).
792 Maximum intensity projections.
793 B) Example of a P079 UBC (soma indicated with O, brush indicated with arrowhead), GRP UBC (soma indicated with
794 *, brush indicated with arrowhead). The GRP UBCs expresses mGluR1 in the somatic membrane and dendritic
795 brush. Most P079 UBCs do not express mGluR1, although some that are weakly labeled do appear to express
796 mGluR1.
797 C) Coronal section of the dorsal cochlear nucleus showing genetically expressed mCitrine (green) from the P079
798 allele, tdTomato (red) from the GRP-Cre/Ai9 alleles, and immunohistochemical labeling of calretinin (magenta).
799 Maximum intensity projections.

800 D) Example of a P079 UBC (soma indicated with O), GRP UBC (soma indicated with *). The P079 UBCs express
801 calretinin in their cytoplasm. GRP UBCs do not express calretinin.
802

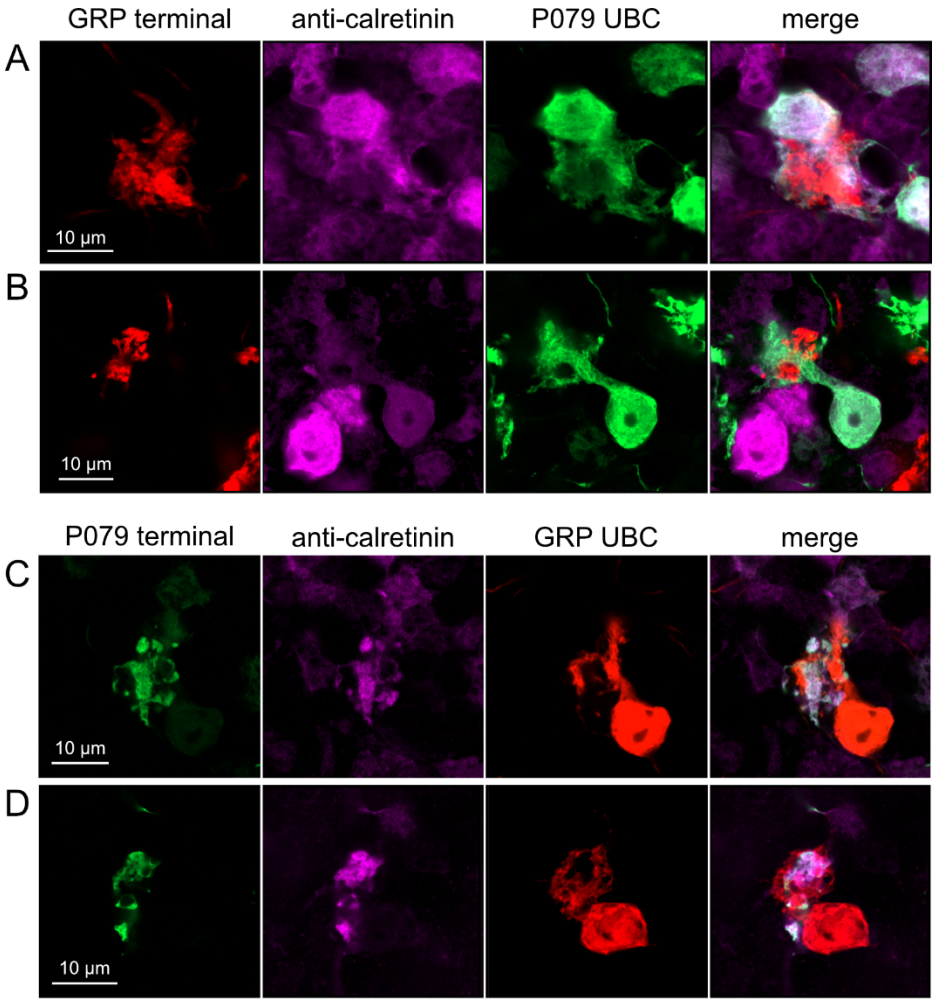

803

804 *Figure 5- Anatomical evidence showing axonal projections between ON and OFF UBC subtype*
805 A-B) ON UBC axon terminals (GRP- red) that project to OFF UBCs (P079- green), confirmed to express calretinin
806 (magenta). Single image sections.
807 C-D) OFF UBC axon terminals (P079- green), confirmed to express calretinin (magenta) contacting the dendritic
808 brushes of ON UBCs (GRP-red). Single image sections.
809

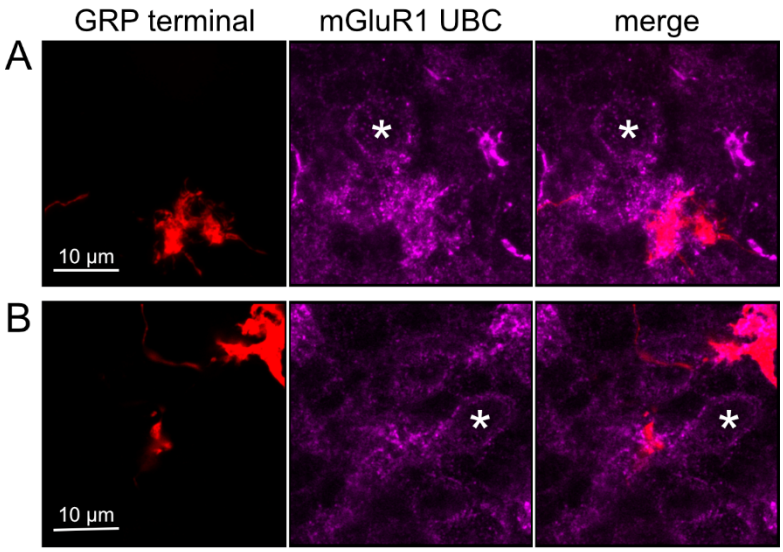

Figure 6- Anatomical evidence for synaptic connections between ON UBCs
A-B) GRP ON UBC terminals (red) contacting mGluR1(+) ON UBCs (magenta). Somas indicated with *. Single image sections.

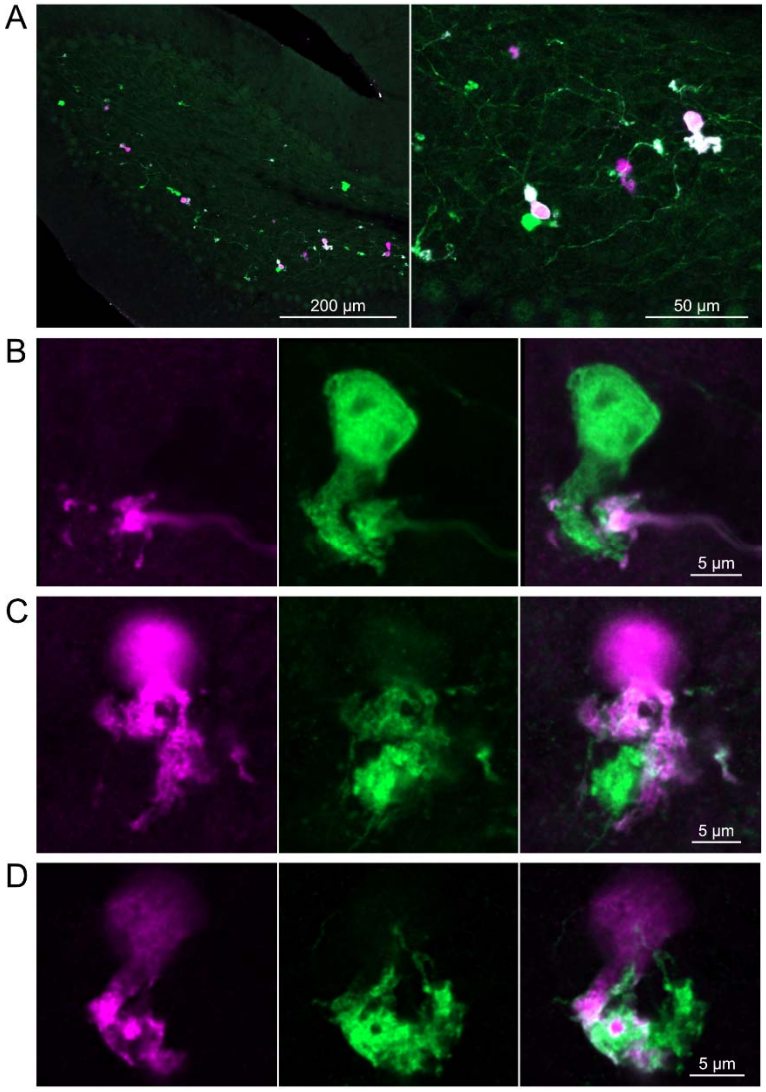

Figure 7- Brainbow reporter labels synaptic connections between GRP ON UBCs
A) GRP ON UBCs expressed fluorescent proteins that were either amplified with the anti-GFP antibody or anti-mCherry antibody. GRP UBCs and their axons and terminals were labeled. Maximum intensity projections.
B) Example of a GRP UBC expressing cytoplasmic YFP (green) that appears to be contacted by a presynaptic terminal from the axon of another GRP UBC that expresses both cytoplasmic YFP (green) and cytoplasmic tdimer2(12) (magenta). Single image sections.
C) Example of GRP ON UBC expressing cytoplasmic tdimer2(12) (magenta) and membrane-bound mCerulean (green) that appears to receive a synaptic terminal that expresses cytoplasmic YFP (green). Single image sections.
D) Example of GRP ON UBC that expresses cytoplasmic tdimer2(12) (magenta) receiving input from a GRP UBC axon that expresses cytoplasmic YFP (green). Single image sections.

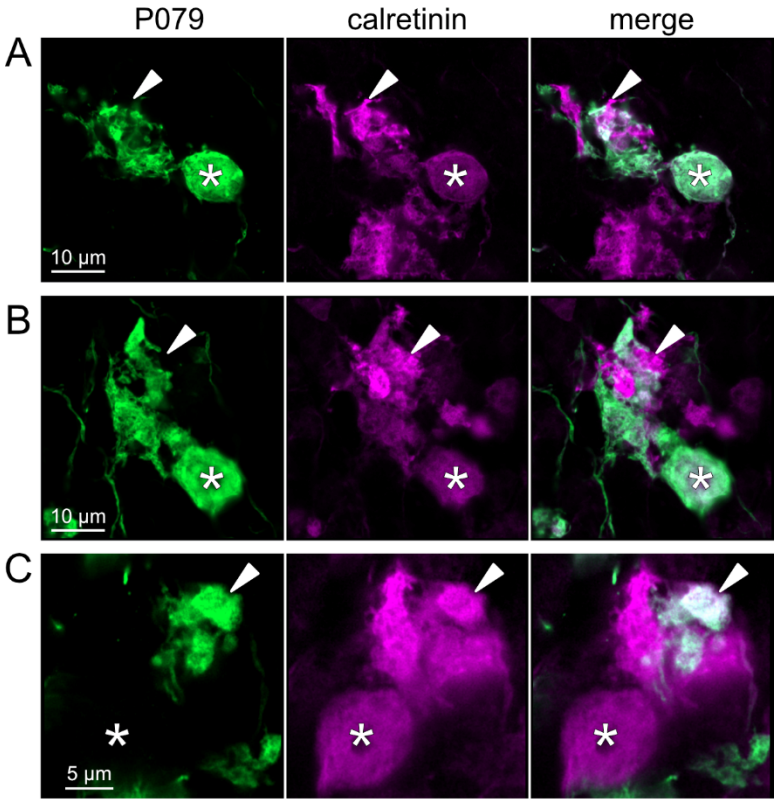

Figure 8- Anatomical evidence for synaptic connections between OFF UBCs

A-B) Examples of P079 OFF UBCs (green) that are confirmed to express calretinin (magenta) and are contacted by calretinin(+) terminals that are not labeled in the P079 line. Single image sections.

C) Example of an OFF UBC that expresses calretinin (magenta) that is contacted by a P079 (green) axon terminal that expresses calretinin (magenta).

Somas are indicated with *, terminals are indicated with arrowheads. Single image sections.

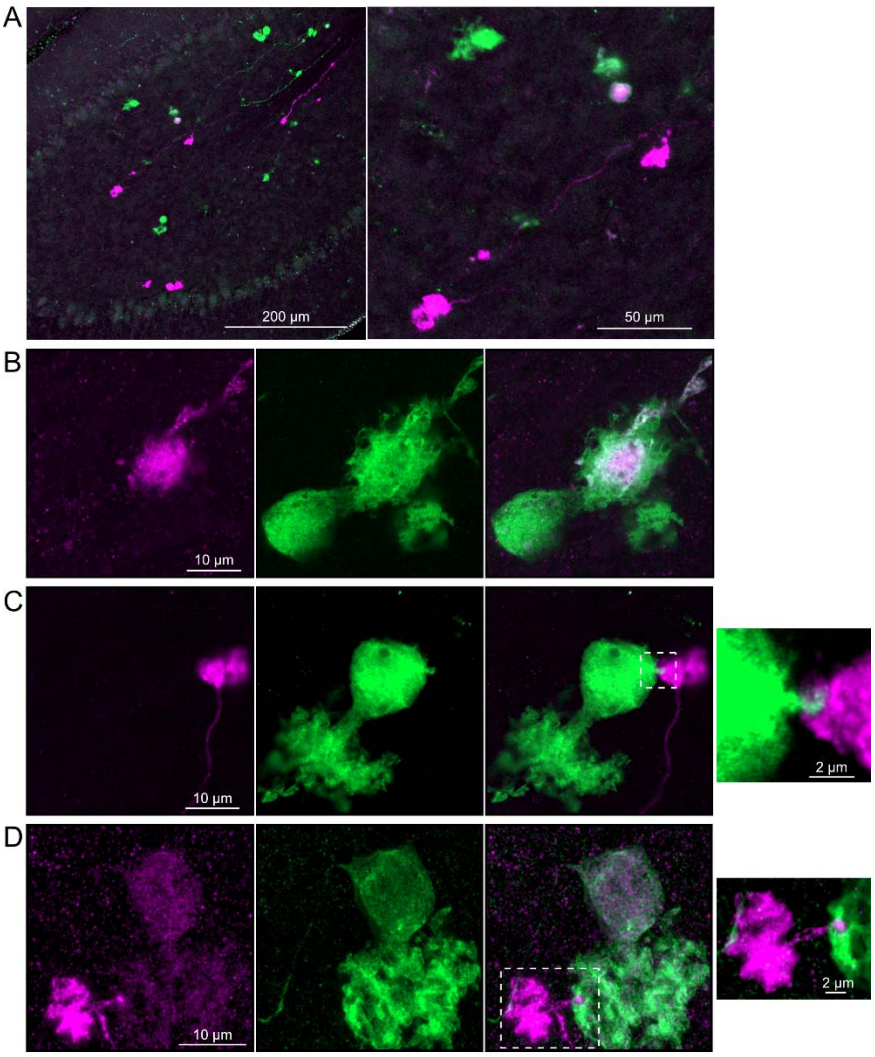

Figure 9- Brainbow reporter labels synaptic connections between OFF UBCs in calretinin-Cre mouse line
A) Calretinin-Cre UBCs expressed fluorescent proteins that were either amplified with the anti-GFP antibody or anti-mCherry antibody, revealing UBCs and their axons and terminals in lobe X. Maximum intensity projections.
B) Example of a labeled calretinin-Cre axon terminal (magenta) that contacted the brush of a calretinin-Cre UBC (green), showing that these OFF UBC project to one another.
C) Example of a calretinin-Cre UBC axon terminal (magenta) that appeared to contact a spine-like extension from the soma of another calretinin-Cre UBC (green).
D) Example of a calretinin-Cre axon terminal (magenta) that projected a small fiber that made a bouton-like synapse onto the brush of another calretinin-Cre UBC (green) that is presumed to have another unlabeled input to the majority of its dendritic brush.

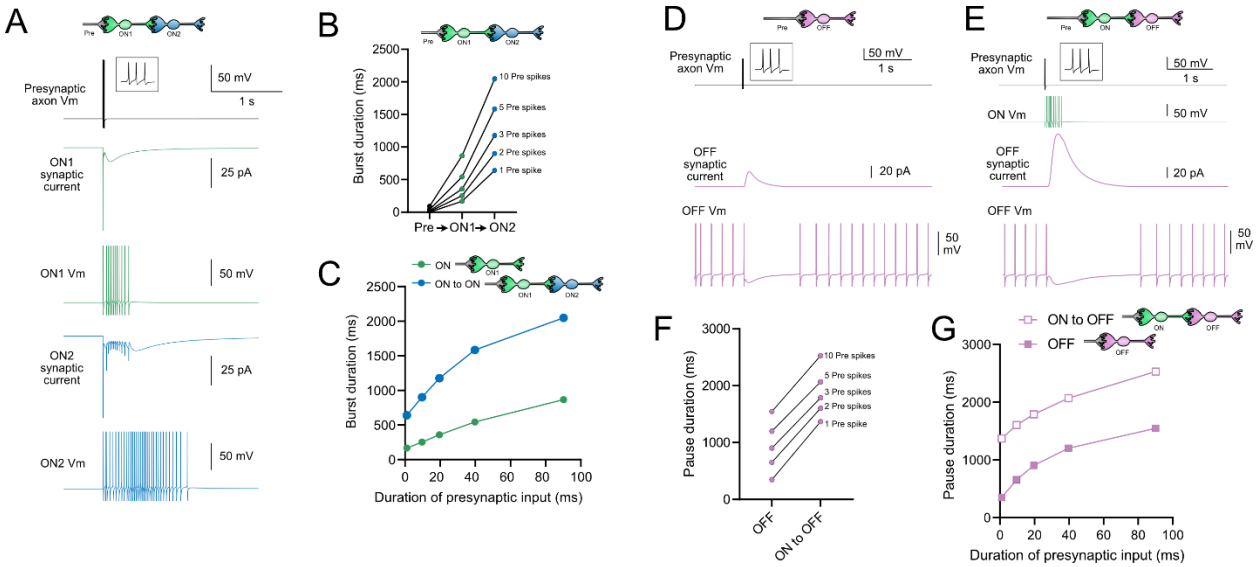

Figure 10- Model predicts that intermediate ON UBCs extend signal

A) Model in which a presynaptic axon fired 3 action potentials (inset shows presynaptic spikes with expanded time scale) that generated an AMPA receptor-mediated synaptic current and a burst in spikes in the first ON UBC (ON1), which produced an extended AMPA receptor-mediated synaptic current in the postsynaptic UBC (ON2) and an extended burst of spikes.

B) Presynaptic spikes were amplified to longer bursts in each subsequent ON UBC.

C) Burst duration in the first ON UBC (green) and second ON UBC (blue) as a function of presynaptic input duration.

D) Model in which a presynaptic axon fired 3 action potentials that generated an mGluR2-mediated synaptic current in an OFF UBC, which produced a pause in spontaneous firing lasting ~1 s.

E) An intermediate ON UBC between the presynaptic axon and OFF UBC generated a larger and longer lasting mGluR2-mediated current that produced an extended pause in spontaneous firing.

F) Pause duration in an OFF UBC was extended by an intermediate ON UBC.

G) Pause duration in an OFF UBC with and without an intermediate ON UBC as a function of presynaptic input duration.

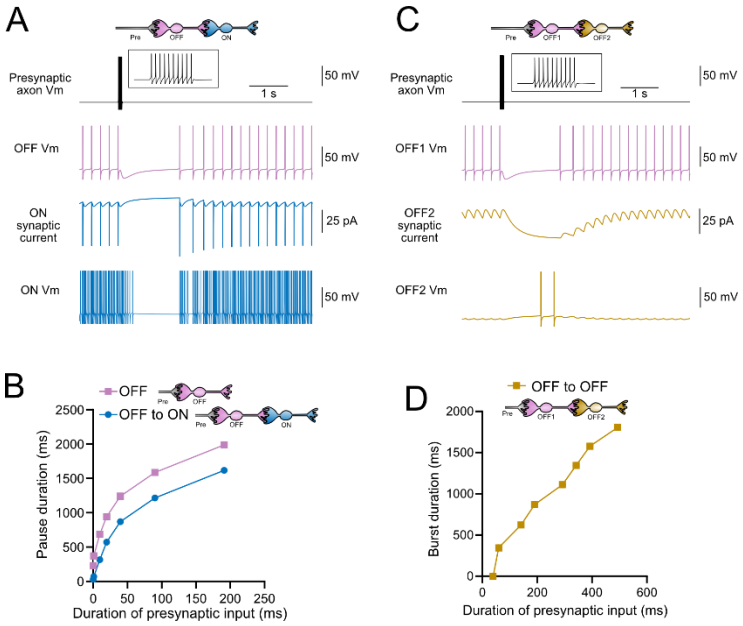

Figure 11- Model predicts that intermediate OFF UBCs delays signals

A) Model showing an intermediate OFF UBC (magenta) that produced a delayed pause in a postsynaptic ON UBC (blue). The spontaneous activity of the intermediate OFF UBC drove irregular spiking in the postsynaptic ON UBC. Presynaptic input (10 spikes shown in inset with expanded time scale) produced a pause in the intermediate OFF UBC, which stopped its release of glutamate onto the ON UBC, and produced a pause after a delay that is due to the slow decay of the AMPA receptor-mediated current.
B) The intermediate OFF UBC (magenta) paused for longer than the postsynaptic ON UBC (blue), because the pause in the ON UBC occurred after a delay and it ended as soon as the intermediate OFF UBC resumed firing.
C) Model showing an intermediate OFF UBC that produced delayed spikes in a postsynaptic OFF UBC. Spontaneous firing of the intermediate OFF UBC (OFF1- magenta) tonically inhibited the postsynaptic OFF UBC (OFF2- gold). Presynaptic input caused a pause in the intermediate OFF UBC, which disinhibited the postsynaptic OFF UBC, allowing it to fire with a delay that depended on the decay of the mGluR2 current.
D) The duration of the burst of action potentials in the postsynaptic UBC increased with longer durations of presynaptic input.

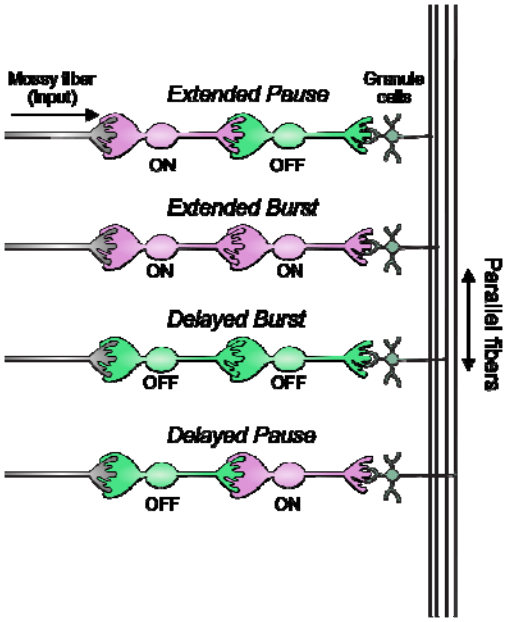

Figure 12- Summary of transformations of spiking patterns in UBC circuits
Four patterns of connectivity between UBC subtypes were anatomically defined and computationally modeled. Intermediate ON UBCs extended the usual pause or burst in firing of the postsynaptic OFF or ON UBC. Intermediate OFF UBCs delayed and inverted the response of the postsynaptic UBC, producing either a delayed burst in OFF UBCs or a delayed pause in ON UBCs.